Forcing Mechanisms of Sea Level Interannual Variability in the Bay of Bengal

WEIQING HAN AND PETER J. WEBSTER

Program in Atmospheric and Oceanic Sciences, University of Colorado, Boulder, Colorado

(Manuscript received 3 July 2000, in final form 21 June 2001)

ABSTRACT

A nonlinear, 4½-layer reduced-gravity ocean model with active thermodynamics and mixed layer physics is used to investigate the causes of sea level interannual variability in the Bay of Bengal, which may contribute to flooding and cholera outbreaks in Bangladesh. Forcing by NCEP–NCAR reanalysis fields from 1958 to 1998 yields realistic solutions in the Indian Ocean basin north of 29°S. Controlled experiments elucidate the roles of the following forcing mechanisms: interannual variability of the Bay of Bengal wind, equatorial wind, river discharges into the bay, and surface buoyancy flux including precipitation minus evaporation (heat fluxes + $P - E$).

Sea level changes in the bay result largely from wind variability, with a typical amplitude of 10 cm and occasionally 10–25 cm at an interannual timescale. Near the eastern and northern boundaries, sea level anomalies (SLAs) are predominantly caused by equatorial wind variability, which generates coastal Kelvin waves that propagate into the bay along the eastern boundary. Near the western boundary the bay wind has a comparable influence as the equatorial wind, especially during the southwest monsoon season, owing to the counterclockwise propagation of coastal Kelvin waves forced by the large-scale alongshore wind stress in the bay. In the bay interior, SLAs are dominated by the equatorial wind forcing in the central bay, result almost equally from the equatorial and the bay wind in the southwestern bay, and are dominated by the bay wind forcing in the southwestern bay during the southwest monsoon. The westward intensification of the bay wind influence is associated with the westward propagation of Rossby waves forced by the large-scale wind curl in the interior bay. The effect of heat fluxes + $P - E$ is generally small. Influence of interannual variability of river discharges is negligible.

SLAs caused by the equatorial wind at the equator and that caused by the bay wind along the northern and western boundaries as well as in the southwestern bay are significantly correlated, reflecting the anomalous wind pattern associated with the dipole mode event in the tropical Indian Ocean. Given the dominance of equatorial wind forcing near the northern bay boundary, SLAs (or alternatively westerly wind anomalies) in the equatorial ocean may serve as a potential index for predicting Bangladesh flooding and cholera.

1. Introduction

For monsoon river delta countries like Bangladesh, which is at or slightly above the sea level, variability of sea level in the Bay of Bengal (hereinafter referred to as the bay) is of some importance and may influence phenomena over a wide range of timescales. For example, on a longer timescale, it is hypothesized that higher sea level tends to retard river water from the Ganges–Brahmaputra complex (which flows through the Bangladesh delta) into the bay, enhancing flooding potential. On a shorter timescale, higher sea level acts to enhance severe flooding during storm surges. In addition, it has been suggested that variability of sea level is correlated with outbreaks of cholera in Bangladesh, because sea surface height may be an indicator for inland incursion of plankton-laden water from the bay, which is a reservoir of the bacteria that cause cholera (Lobitz et al. 2000). Understanding interannual variability of sea level in the Bay of Bengal, therefore, may be an important step toward predicting flooding and epidemic cholera in monsoon river deltas.

Since the ocean and the atmosphere are a coupled system, variability of sea level reflects changes in climate. One of the most important aspects of the climate in the bay is the Indian monsoon, which possesses large interannual variability. This variability may cause marked sea level change due to fluctuation of monsoon wind, precipitation minus evaporation ($P - E$), heat fluxes, and river runoff into the bay. There are also potential remote influences. Sea level signals driven by the equatorial wind can propagate into the bay as coastal Kelvin waves and westward radiating Rossby waves, each of which has a sea level signature that may impact the sea level in the bay.

a. Background

There are a few earlier studies on interannual variability of sea level in the Indian Ocean. For example, Perigaud and Delecluse (1993) discussed Indian Ocean

Corresponding author address: Dr. Weiqing Han, Program in Atmospheric and Oceanic Sciences, University of Colorado, Campus Box 311, Boulder, CO 80309-0311.
E-mail: whan@monsoon.colorado.edu

sea level interannual variability using Geosat satellite altimeter data for the period of April 1985–September 1989 and sea level variability calculated from the solution to a 1½-layer model. Their results showed a striking difference between observed and simulated sea level anomalies (SLAs) in the bay, owing to a combination of accumulated errors in the satellite observations and the simplicity of the model. The model had only one active layer, and it also lacked thermal forcing, salinity, and river runoff, all of which can potentially affect sea level change in the bay. These problems are acknowledged by Perigaud and Delecluse (1993).

Clarke and Liu (1994), using monthly Indian and Pakistani sea level records together with a simple linear inviscid model, examined sea level interannual variability along the coasts of northern Indian Ocean. They suggested that sea level change along at least 6000 km of Indian Ocean coastline from the equator to Bombay is generated remotely by interannual variability of zonal winds along the equator. They found spatially varying boundary signals forced by the coastal alongshore wind stress to be negligible. The influence of remote equatorial forcing on the bay circulation has already been pointed out by Yu et al. (1991), Potemra et al. (1991), and McCreary et al. (1993, 1996). Shankar and Shetye (1999) suggested that interdecadal variability of sea level at Bombay mimicked the variability in rainfall over the Indian subcontinent. They hypothesized that the seasonal river outflow of the monsoon rainfall into the seas around India, and the dynamics of currents along the Indian coast, provide links between the rainfall over the Indian subcontinent and the sea level along the coast of India, with coastal salinity playing an intermediate role.

b. Goal

The goal of this research is to examine how important each of the suite of candidate mechanisms is in causing interannual sea level changes in the bay. These mechanisms are interannual variability of river discharges into the bay, the local bay wind, remote equatorial wind, and surface buoyancy flux including $P - E$ (heat fluxes $+ P - E$). To make a systematic assessment of the role of each mechanism, a series of experiments is undertaken using an intermediate ocean model. Accomplishment of this research will not only improve our understanding of important mechanisms that determine interannual variability of sea level in the bay, but also potentially contribute to predicting flooding and cholera in river delta countries around the bay, such as Bangladesh.

The paper is organized as follows. Section 2 describes the ocean model, forcing, and design of experiments; section 3 compares solution MR with the observations; section 4 reports interannual variability of sea level from the experiments; section 5 provides a summary and discussion.

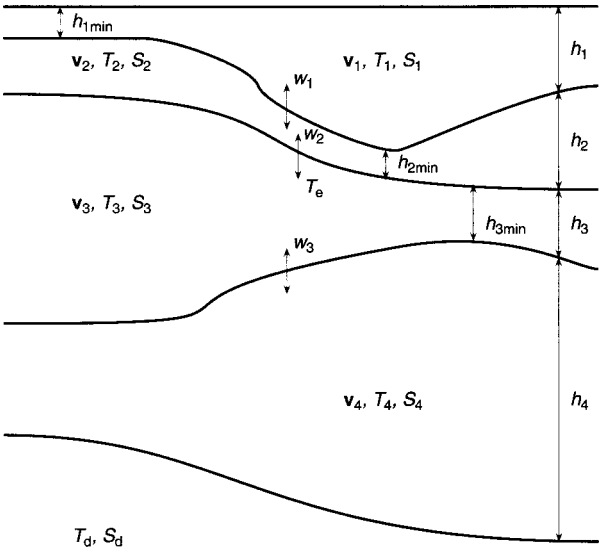

FIG. 1. A schematic diagram illustrating layer structure of the 4½-layer ocean model.

2. Ocean model

a. Model description

The model used in this study is a 4½-layer, reduced-gravity system (Fig. 1). It consists of four active layers with thicknesses h_i ($i = 1$–4 is a layer index), temperatures T_i, salinities S_i, and velocities $\mathbf{V}_i = (u_i, v_i)$, overlying a deep, quiescent ocean with temperature T_d and salinity S_d, where pressure gradients are assumed to vanish (the "½" layer). The w_i terms are velocities at the bases of layers 1–3 that specify how water transfers across the interfaces between the layers, and they are described in detail in Han et al. (1999) and Han (1999). The specification of w_i ensures that layer thicknesses h_1, h_2, and h_3 are greater than or equal to their minimum values $h_{1min} = h_{2min} = 10$ m and $h_{3min} = 50$ m. Temperature T_e, rather than T_3, is entrained from layer 3 to layer 2, as discussed in McCreary et al. (1993).

The T_i and S_i fields are allowed to vary in response to both surface forcing and across-layer transfer by the w_i fields, so the layers are not isopycnal ones. Rather, it is more appropriate to interpret them as corresponding to distinct water mass types, namely, the surface mixed layer, seasonal thermocline, thermocline, and upper-intermediate water in layers 1–4, respectively. The model sea level d is determined by

$$d = \frac{1}{\rho_0} \sum_{i=1}^{4} (\rho_d - \rho_i) h_i, \tag{1}$$

where

$$\rho_i = \rho_0 (1 + \alpha_t T_i + \alpha_s S_i) \tag{2}$$

is the density of layer i and of the deep ocean (with subscript i replaced by d), $\rho_0 = 1$ g cm^{-3}, $\alpha_t = -2.5 \times 10^{-4}$ °C^{-1}, and $\alpha_s = 8 \times 10^{-4}$ psu^{-1}. Details of the

dynamic, thermodynamic, and salinity equations are discussed in Han (1999), Han and McCreary (2001), and Han et al. (2001).

b. Basin and boundary conditions

The model basin resembles the actual Indian Ocean north of 29°S and is shown in the left panels of Fig. 3, which is comparable with the more accurate basin geometry shown in the right panels. All the continental boundaries (including the islands) are vertical walls, and no-slip boundary conditions are applied. An exception to this boundary condition is for the consideration of river runoff, where freshwater influxes are specified at locations corresponding to the rivers (see Han and McCreary 2001). The southern boundary is open and zero-gradient boundary conditions with a damper on u_i are applied (see McCreary et al. 1993). An exception is that, for the situation when there is flow entering the basin ($v_i > 0$ at $y = 29°$S), we specify the inflow temperature and salinity values to be the annual and zonal mean temperatures and salinities of Levitus and Boyer (1994) and Levitus et al. (1994) climatologies. Interested readers may consult McCreary et al. (1993) and Han (1999) for more details.

c. Forcing and numerics

1) NCEP FORCING

Surface forcing fields used to drive the model are either directly from (e.g., precipitation) or derived from (e.g., wind stress, heat fluxes, and evaporation) the National Centers for Environmental Prediction–National Center for Atmospheric Research (NCEP–NCAR) monthly mean reanalysis from 1958 to 1998. The wind, air temperature, and specific humidity are at the 1000 hPa level; the solar shortwave radiation, outgoing longwave radiation, and precipitation are at the surface level. The wind stress, $\boldsymbol{\tau} = \rho_a C_D |\mathbf{V}| \mathbf{V}$, is calculated from the wind speed, $\mathbf{V}$, with $\rho_a = 0.001175$ g cm^{-3} and $C_D = 0.0015$. The sensible and latent heat fluxes as well as evaporation are determined from standard bulk formulae (McCreary and Kundu 1989; McCreary et al. 1993). Solar radiation is allowed to penetrate down through the surface mixed layer to the deeper layers in the model, as described by Han et al. (2001). The NCEP monthly mean climatological forcing fields are mean values calculated for the period 1958–98.

Modifications have been made to the NCEP forcings. First, due to the difference of the basin configurations and horizontal grid resolutions between our model and the NCEP data, certain land values in the forcing fields extend to the ocean basin near the model boundaries. These land values are replaced by the adjacent ocean data. Second, we reduce the NCEP wind speed and incoming solar radiation to 90% of their original values, and increase the specific humidity by 20% north of 20°N and south of 15°S with a ramp of 5° (15°–20°N and 10°–15°S). These adjustments are made by comparing the NCEP climatologies with the climatological data derived by Rao et al. (1989, 1991) from the Comprehensive Oceanographic and Atmospheric Data Set (COADS).

2) RIVER FORCING

Three major rivers are included: the Ganges–Brahmaputra, Irrawaddy, and Godavari. Their locations in the model are 20°N, 88°–90°E; 17°–15.5°N, 94.5°–96.5°E; and 16°–17°N, 83.5°–84.5°E respectively.

The observed monthly discharges for the Ganges–Brahmaputra during 1969–75 are from UNESCO (1993), with missing data for the period of April 1971–March 1972. The missing values are estimated by linear interpolating the discharge data between the corresponding months of the two adjacent years. For other years within the period of 1958–98, the discharges are estimated by the NCEP precipitation in the catchment of the Ganges–Brahmaputra, a region defined to be (22.5°–31°N, 76°–96°E) in this paper, as suggested by Huq et al. (1999; their Fig. 2). The estimation is based on the fact that discharge of the Ganges–Brahmaputra is determined from the precipitation in its catchment. The correlation between the monthly NCEP rainfall in the catchment and the Ganges–Brahmaputra discharge for the period of 1969–75 is 0.90, 0.96, and 0.94, respectively, when the monthly rainfall of the present month, present plus previous, and present plus previous two months is used in calculating the correlations. The significance level for the correlations is above 99.5%. These high correlations suggest that NCEP rainfall is reasonable to use for the estimation, and the increase of correlation when the rainfall from both the present and previous months is used indicates the memory for the precipitated water to make its way into the ocean. Thus, the present plus previous month precipitation, which gives the highest correlation, is used for estimating the river discharges.

First, linear regression is performed between the observed river discharge and the NCEP precipitation in the catchment to obtain the coefficients for the linear fit. Then, monthly discharges for years of no observations are reconstructed by inserting the catchment rainfall values in the regression equation. Due to the lack of discharge data for river Irrawaddy, a 40% of Ganges–Brahmaputra discharge is used (S. Shetye 2001, personal communication).

River Godavari has a 17-yr observed monthly record: 1958–60, 1965–74, and 1976–79. The catchment of the Godavari is defined to be (16°–22.5°N, 75°–85°E) in this paper. Different regions have also been tested, and the current one gives the highest correlation (0.83) between the catchment rainfall of the present plus previous month and the river discharge, with a significance level of above 99.5%. This lower correlation relative to that

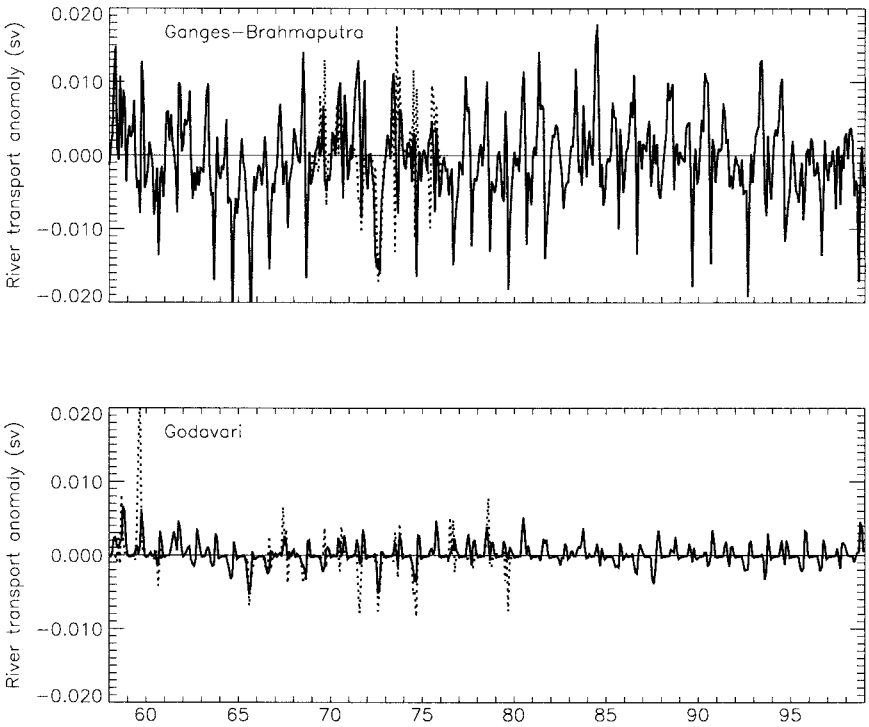

FIG. 2. Interannual variability of estimated (solid lines) and observed (dashed lines) discharges (Sv) for the rivers Ganges–Brahmaputra (top) and Godavari (bottom) during 1958–98. The climatological annual cycle for each river is removed from both the observation and estimation.

of the Ganges–Brahmaputra might result from the NCEP rainfall error in the Godavari catchment. Similar to river Ganges–Brahmaputra, discharges of the Godavari during years of no observations for the period of 1958–98 are estimated by performing linear regression between the catchment rainfall and the discharge.

Monthly climatologies for the rivers Ganges–Brahmaputra (Fig. 4 of Han and McCreary 2001) and Godavari (not shown) are the mean values calculated from their available data records. Climatology for the Irrawaddy is chosen to be 40% of that for the Ganges–Brahmaputra.

Figure 2 shows the interannual variabilities (with the observed monthly climatology removed) of the estimated (solid lines) and observed (dashed lines) discharges for the Ganges–Brahmaputra (top panel) and the Godavari (bottom panel) during 1958–98. Basically, the estimated discharges are able to describe the observed interannual variabilities, although their amplitudes might be underestimated during some years (compare the solid and dashed lines in each panel). River discharges used to force the model are the observed values when the data are available and reconstructed values for the years of no observations with their observed monthly climatologies included. Forcing due to each river is simulated by specifying lateral boundary conditions at the corresponding location, as described in detail by Han and McCreary (2001).

3) NUMERICS

We first spin up the model for 30 years using the monthly NCEP and river discharge climatologies. Based on the climatological state, we force the model by monthly NCEP reanalysis and river discharges from 1958 to 1998. The horizontal resolution of the grid is $\Delta x = \Delta y = 55$ km and the time step is $\Delta t = 0.8$ h. Parameters utilized in our model and other numerical details can be found in McCreary et al. (1993) and Han et al. (1999). One difference is the mixing coefficient for layer thickness, which is increased from the 1×10^7 cm^2 s^{-1} in the above studies to 5×10^7 cm^2 s^{-1} in the current research in order to reduce the noise in the h_i field for the interannual runs.

d. Design of experiments

In this section, we design a hierarchy of solutions used to isolate each candidate mechanism that may be influential in producing sea level variability in the bay.

- Solution background run (BR) is a climatological solution forced by river and NCEP monthly climatologies. This solution describes the mean annual cycle of sea level and serves as an initial condition and a reference for the interannual runs. Unless specified otherwise, SLAs in the interannual solutions are anomalies from solution BR.

- Solution main run (MR) is forced by all interannual forcings: river discharge, wind stress (the bay wind + equatorial wind), and heat fluxes + $P - E$. It is the most complete solution in our hierarchy. All the test solutions below are stripped down from the MR.
- Solution test run 1 (TR1) is the same as the MR, except for using climatological river discharges. The difference solution, MR − TR1, estimates the sea level change caused by interannual variability of river runoff.
- Solution test run 2 (TR2) is the same as the MR except for using climatological wind stress. The difference solution, MR − TR2, measures the influence of wind variability.
- Solution test run 3 (TR3) is the same as the MR except for the use of climatological precipitation and other climatological atmospheric variables to calculate surface heat fluxes and evaporation. The difference solution, MR − TR3, estimates forcing due to heat fluxes + $P - E$.
- Solution test run 4 (TR4) is the same as the MR, except for using climatological wind stress in the bay (7°–20°N, 80°–97°E) and ramping it to the interannual values within 3° south of 7°N and 2.5° west of 80°E. The difference solution, MR − TR4, assesses the impact of Bay of Bengal wind forcing.
- Difference solution, TR4 − TR2, estimates the influence of equatorial wind variability, because the only difference between the two solutions is that the former is forced by interannually varying wind outside the bay, whereas the latter is driven by the wind climatology.

Note that in all solutions, the model sea surface temperature (SST) is used to calculate surface heat fluxes and evaporation. The feedback of SST to heat fluxes and evaporation, therefore, is included in each solution.

3. MR and observations

Figure 3 shows the monthly mean SLA for November 1996 (peak of a negative dipole), November 1997 (peak of a positive dipole), and August 1998 (Bangladesh flooding and high cholera during a negative dipole) from solution MR (left panels) and from TOPEX/Poseidon satellite altimeter data (right panels). The three years are chosen within the period of 1993–98, when TOPEX data are available during our interested period. The dipole is defined to be an anomalous climate state in the tropical Indian Ocean when the SST is colder than usual near Sumatra and warmer than usual in a large region of the western basin (Webster et al. 1999; Saji et al. 1999; Murtugudde et al. 2000; Yu and Rienecker 1999, 2000; Behara et al. 1999). It usually begins when the southwestern monsoon commences and reaches its maximum amplitude during fall. An opposite situation is referred to as a negative dipole when the SST is anomalously warm near Sumatra and anomalously cold in the western tropical Indian Ocean. Its strength is measured by the dipole mode index, which is defined as the difference of mean SST anomaly (SSTA) during September, October, and November between the tropical western (10°S–10°N, 50°–70°E) and the tropical southeast Indian Ocean (10°S–0°, 90°–110°E), regions applied by Saji et al. (1999). Figure 4 shows the dipole mode index calculated from the monthly Reynolds SST data (dashed line: Reynolds and Smith 1994) and from solution MR (solid line) for the period of 1958–98, indicating a strong negative dipole in 1996, a positive dipole in 1997, and a moderate negative dipole in 1998. Our model captures all dipole mode events that occurred in the data, and the correlation between the model and data dipole mode index is 0.91 with a significance level of above 99.5%.

The TOPEX data is from the University of Texas Center for Space Research (http://www.csr.utexas.edu) with 1° × 1° resolution and a 10-day cycle. There are two missing cycles, each of which is estimated by linear interpolating values of its two adjacent cycles. The monthly mean is performed for the TOPEX data to be consistent with our model solution. The modeled and observed mean sea levels for the period of 1993–98 are removed from the model and data, respectively. Their mean annual cycle, however, are retained in the SLAs shown in Fig. 3.

In all three years, SLAs in our MR agree reasonably well with the TOPEX data, with a positive SLA in the eastern tropical ocean during a negative dipole (top panels) and a negative SLA in the same region during a positive dipole (middle panels). Associated with the positive dipole, there is a sea level high in the southern tropical ocean at 5°S–15°S, as discussed by Webster et al. (1999). During the negative dipole of 1998 (bottom), SLA is positive in the eastern tropical ocean in August, negative near the southern and western Indian coasts, negative in the southeast Indian Ocean, and positive in the central-western tropical ocean. In the Arabian Sea and the Bay of Bengal, the model SLAs also agree with the data.

There are, however, some differences in amplitudes between the model solution and the observation. These differences are most likely because of the inaccuracy of NCEP forcings and the simplicity of the model. Tests of different wind products suggested that the Florida State University winds produce a better SST anomaly, and therefore a better SLA, than the NCEP winds in the tropical Indian Ocean during dipole years (A. Schiller 2000, personal communication). In addition, our model is a 4½-layer reduced gravity system. It filters out the barotropic mode, adopts the Boussinesq approximation, and has only 4 degrees of freedom in the vertical direction, all of which may affect the amplitude of sea level variability. In the coastal regions of the bay, however, the model solution tends to resolve the structure of coastal Kelvin waves better than the data. This is because the horizontal resolution of our model is 0.5° × 0.5°, whereas that of the TOPEX data is 1° × 1°.

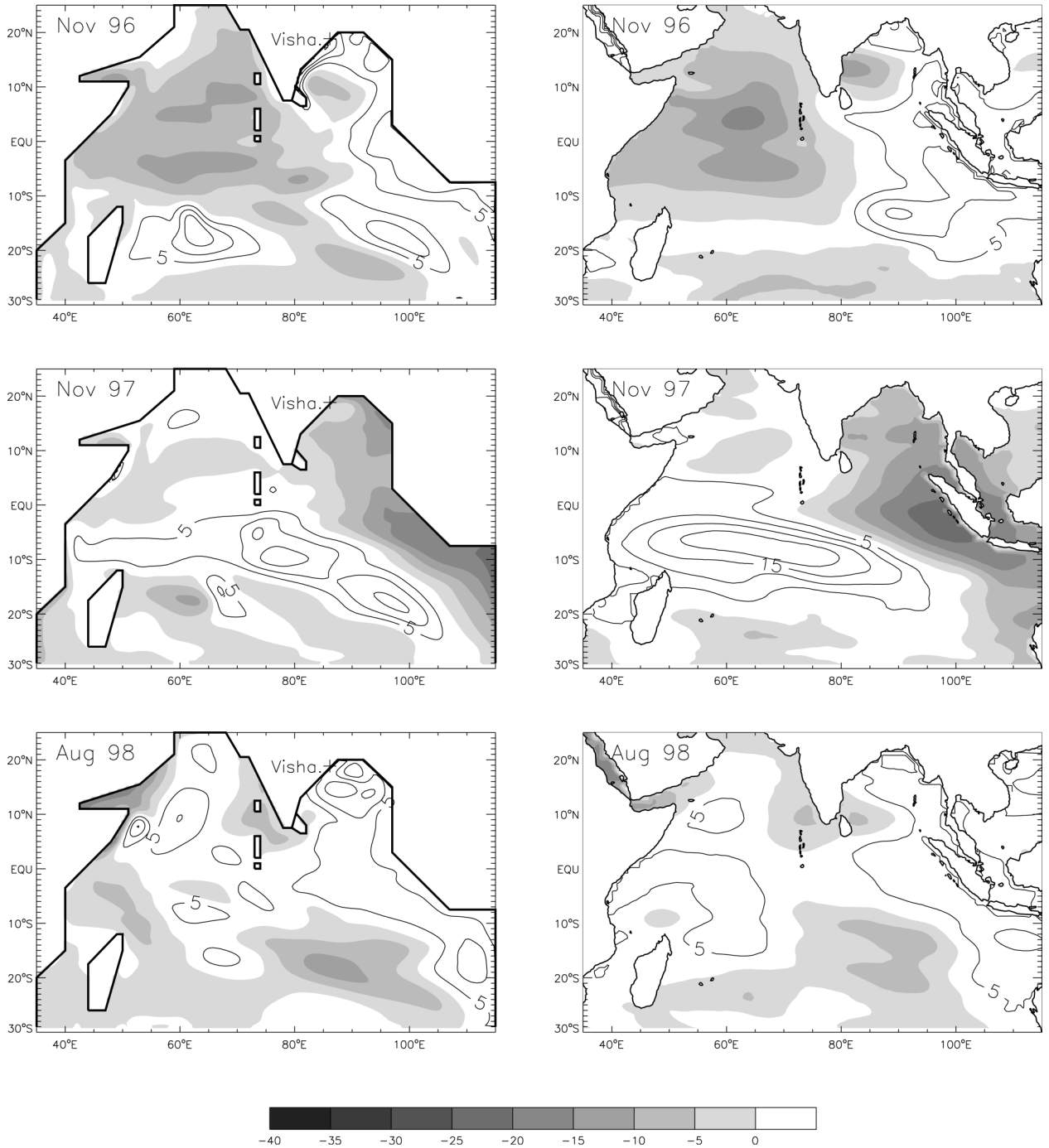

FIG. 3. Sea level anomaly for Nov 1996 (top), Nov 1997 (middle), and (bottom) Aug 1998 from solution main run (MR: left) and from TOPEX/Poseidon altimeter data (right). Positive values are contoured and negative values are shaded, with an interval of 5 cm. The location for sea level station Vishakhaptnam, discussed in Fig. 5, is indicated by "+" in the left panels.

Additionally, a significant amount of data was lost in coastal regions due to the lack of accurate tide models (S. Bulusu 2001, personal communication).

To further confirm our model performance along the coast in the northern bay, where sea level is suggested to play a role in causing outbreaks of cholera and is hypothesized to be potentially important in enhancing the flooding potential in Bangladesh, Fig. 5 shows the annual mean SLA from solution MR (solid line) and from the tide gauge data (dashed line) at station Vishakhaptnam for the period of 1958–89, when the data is available. The geographic location for Vishakhaptnam

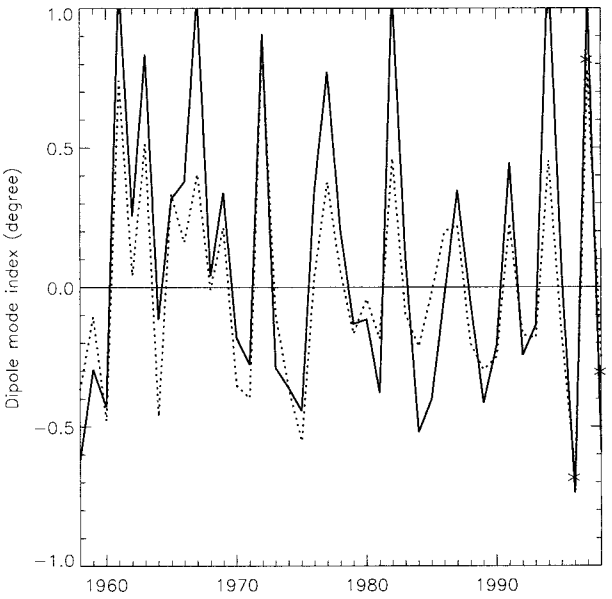

FIG. 4. Time series of the dipole mode index (°C) from 1958 to 1998, which is defined as the difference of the mean SST anomaly of Sep, Oct, and Nov between the tropical western (10°S–10°N, 50°–70°E) and southeast (10°S–0°, 90°–110°E) Indian Ocean calculated from monthly Reynolds SST (dashed line) and from solution MR (solid line). Asterisks indicate the three years discussed in Fig. 3.

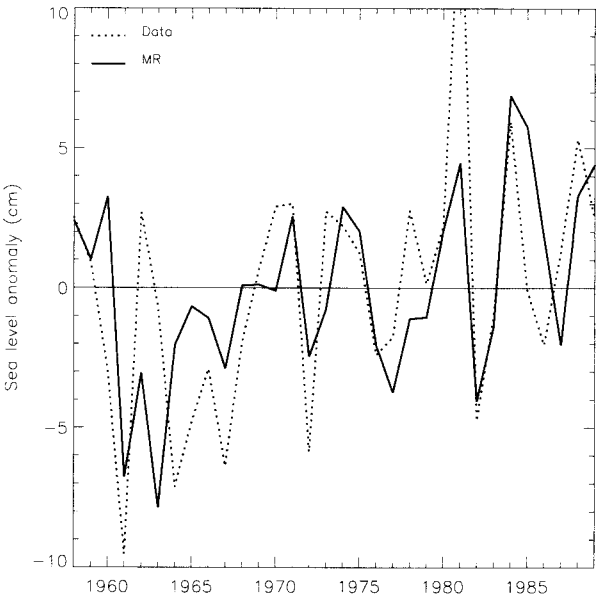

FIG. 5. Observed and modeled sea level interannual variability (cm) from 1958 to 1989: Permanent Service of Mean Sea Level (PSMSL) data corrected by the COADS atmospheric pressure (dashed curve) and solution MR (solid curve) at Vishakhaptnam.

is indicated by the plus sign in the left panels of Fig. 3. The mean sea levels for 1959–89 are removed from both the solution and the data. Generally, our MR reproduces the sea level interannual variability present in the observation, although the amplitudes tend to be underestimated during some years. The correlation between the SLA from solution MR and that from the data is 0.6, with a significance level of above 99.5%.

The good agreement between our MR solution and the observations (Figs. 3–5) gives us confidence that the model properly represents fundamental physics that determine sea level variability both within and outside the bay.

4. Interannual variability

In this section, we first describe the climatological annual cycle of sea level in the bay (section 4a), which provides a reference for sea level interannual variability. Then we report interannual variability of sea level from solution MR and assess the contribution due to each candidate mechanism (section 4b). In section 4c we discuss the dynamical processes that account for the wind-induced sea level variability, in section 4d we perform spectral analysis on SLAs and point out the dominant sea level oscillations, and finally in section 4e we discuss the potential application of this research in predicting Bangladesh flooding and cholera.

a. Climatological annual cycle

Figure 6 provides an overview of the sea level climatological annual cycle from solution BR. Unless specified, all SLAs discussed in later sections are the anomalies from this mean annual cycle. Dynamics of the sea level annual cycle in the bay have been discussed by McCreary et al. (1996), and the influence of the bay rivers on the annual cycle of sea level has been described by Han et al. (2001). Here then we only provide a brief discussion. To quantify the influence of the bay rivers on the mean annual cycle of sea level, we find another solution that is the same as the BR except for excluding the bay rivers (not shown). Discussions below are based on comparisons between this solution and the BR.

During the northeast monsoon, the northeasterly wind adjacent to the east coast of India (not shown) produces a coastal downwelling, raising the sea level by 2–6 cm along the east Indian coast (January panel). At the same time and in the same region, freshwater from the rivers increases the sea level by 2–4 cm, owing to the river water being advected southward by the East India Coastal Current (EICC) as a coastal plume (see Shetye 1993; Han et al. 2001). The negative SLA in the eastern and northern bay is caused by coastal Kelvin waves associated with a low sea level, which is originated from the eastern equatorial ocean because the equatorial easterly wind during winter generates an equatorial divergence and shallows the thermocline, and therefore decreases the sea level.

From February to April, negative wind curl in the central and western bay produces a high sea level, es-

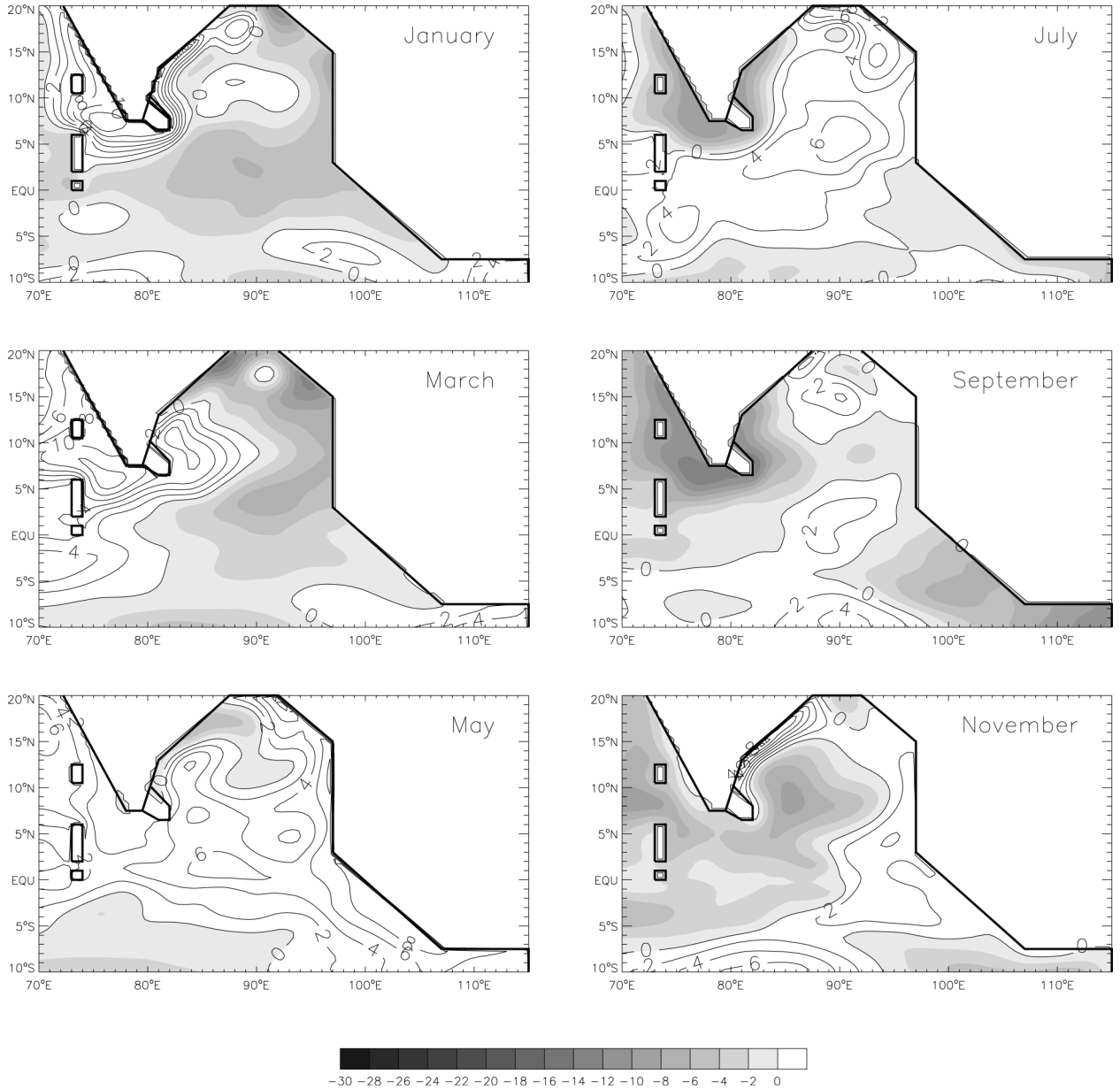

FIG. 6. Bimonthly plot of sea level annual cycle from solution background run (BR), which represents the climatological annual evolution of sea level. It is obtained by subtracting the annual-mean sea level from the value of each month. Positive values are contoured and negative values are shaded, with an interval of 2 cm.

pecially in the southwestern bay (March panel). The negative SLA in the eastern and northern bay strengthens and extends farther along the coast and to the bay interior due to coastal Kelvin waves and westward propagating Rossby waves.

In May, a high sea level pattern presents in the eastern equatorial ocean due to the eastward propagation of equatorial Kelvin waves associated with a high sea level. The strong equatorial westerly winds during April and May cause equatorial convergence, deepen the thermocline, and increase the sea level. In addition, the spring Wyrtki jet acts to pile up water in the eastern basin, contributing to the sea level increase. This high sea level signal with an amplitude of 2–6 cm propagates into the eastern and northern bay as coastal Kelvin waves, and it also radiates westward from the eastern boundary into the bay interior as Rossby waves, raising the sea level in the eastern, northern, and central bay from May to July. During the same period the bay rivers have significant discharges, increasing the sea level by 2–6 cm in some regions of the bay (not shown). From July to September, the southwest monsoon wind gen-

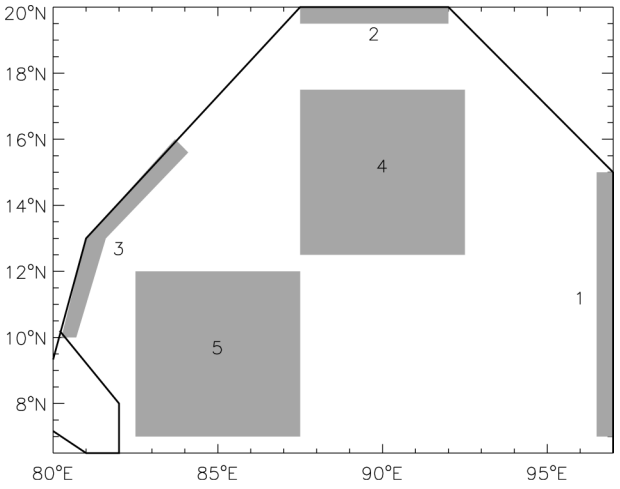

FIG. 7. Five regions in the bay where time series of area-mean SLAs will be shown. Regions 1–3 represent the coastal regions of the bay: eastern, northern, and western boundaries. Regions 4–5 represent the bay interior: central and southwestern bay.

erates coastal upwelling, causing a low sea level along the east Indian coast. At the same time, sea level in the eastern equatorial ocean decreases, due to the relaxation of equatorial westerly wind.

In the following season, a low sea level presents in the bay interior due to the positive wind curl north and east of Sri Lanka (November panel). Along the western and eastern boundaries, however, positive SLAs occur. The high sea level signal with an amplitude of 10 cm along the east Indian coast results primarily from the freshwater plume (6 cm) and from forcing by the northeasterly monsoon wind causing a coastal downwelling (4 cm). As in May, the positive SLA in the eastern bay during November is caused by coastal Kelvin waves originated from the eastern equatorial ocean, where the strong equatorial westerly wind during fall and the fall Wyrtki jet produce a high sea level.

b. MR and solutions due to each mechanism

Figure 7 shows five representative regions in the bay where the solutions will be discussed. Regions 1–3 correspond to the eastern, northern, and western boundaries of the bay, respectively, which sometimes are referred to as the eastern, northern, and western bay in the text. Regions 4–5 represent the bay interior (the central and southwestern bay).

1) COASTS

Along the coasts (regions 1–3 of Fig. 7), sea level interannual variability generally attains a value of −15–10 cm (thick solid lines of Figs. 8a–c). Occasionally SLAs can be as large as −25 cm in the western bay, such as during October of 1961 (bottom panel of Fig. 8c). In the eastern bay (Fig. 8a), SLAs are dominated by the equatorial wind forcing throughout the year (medium solid lines), and influence of the bay wind is generally smaller than 2 cm (thin solid lines). As in the eastern bay, SLAs in the northern bay (Fig. 8b) are predominantly caused by equatorial wind variability. Amplitudes of SLAs produced by the bay wind, however, increase compared to their values in the eastern bay. Near the western boundary, SLAs forced by the equatorial wind are large (Fig. 8c), but the bay wind generates SLAs with comparable amplitudes especially during summer and fall (lower-middle and bottom panels). Compared to solution MR, influence of the equatorial wind forcing decreases progressively from the eastern, via northern, to the western bay, whereas effect of the bay wind increases with its maximum influence occurring during summer and fall, as can be visually identified in Figs. 8a–c (lower-middle and bottom panels) and will be explained in section 4c.

Based on the 41-yr monthly results, cross correlations between SLAs from solution MR and from the solution forced by the equatorial wind are 0.95, 0.93, and 0.82 in the eastern, northern, and western bay, respectively, with a significance level of above 99.5% (see Table 1). Unless specified otherwise, all significance levels discussed in this paper are above 99.5%. Ratios of standard deviation between SLAs forced by the equatorial wind and that from the MR are 0.95, 0.85, and 0.75 in the three regions, respectively (values in the brackets of Table 1). The strong correlation and high percentage of standard deviation suggest that SLAs generated by the equatorial wind not only are in phase with, but also explain most amplitudes of sea level variabilities in, solution MR, especially in the eastern and northern bay as demonstrated by Figs. 8a–c and suggested by Clarke and Liu (1994). The correlations and deviation ratios, however, decrease by a significant amount from the eastern via northern to the western bay, owing primarily to the increasing importance of the bay wind rather than to the decreasing amplitudes of SLAs forced by the equatorial wind. Indeed, correlations between the MR and the solution forced by the bay wind are 0.28, 0.57, 0.71, and ratios of standard deviation are 0.26, 0.40, 0.59 in the eastern, northern, and western bay, respectively (Table 1), demonstrating the increasing importance of forcing due to the bay wind as shown in Figs. 8a–c.

In the eastern bay, SLAs in solution MR are produced primarily by the equatorial wind in all seasons of a year, and influence of the bay wind is negligible. In the northern bay, there is a significant contribution from the bay wind during summer (June–August) and fall (September–November), with correlation coefficients (ratios of standard deviation) with the MR being 0.67 and 0.66 (0.48 and 0.44), respectively, compared to 0.906 and 0.905 (0.74 and 0.86) for the equatorial wind forcing. The dominance of equatorial wind in causing sea level interannual variability along the eastern and northern boundaries of the bay agrees with Clarke and Liu

(1994), who suggested that interannual variability of sea level along at least 6000 km of the north Indian Ocean coastline from the equator to Bombay is generated by equatorial wind variability, and effect of the alongshore wind stress is negligible. In contrast to Clarke and Liu (1994), our solutions suggest that influence of the bay wind is comparable with that of the equatorial wind along the western boundary, especially during summer and fall when correlation coefficients (ratios of standard deviation) are 0.81 and 0.84 (0.59 and 0.57) for the bay wind and 0.86 and 0.92 (0.57 and 0.65) for the equatorial wind forcing.

Influence of the rivers is negligible (thick dashed lines in Figs. 8a–c; Table 1). It causes a maximum SLA of about 1 cm during the southwest monsoon in the northern bay such as during 1964 and 1984 (July panel of Fig. 8b), when the discharge of river Ganges–Brahmaputra (Fig. 2) is 24% lower (1964) or 22% higher (1984) than its peak discharge of 0.082 Sv (Sv $\equiv$ 106 $m^3\ s^{-1}$) in the climatology (Fig. 4 of Han and McCreary 2001). Although sea level changes caused by including the climatological rivers are large, SLAs produced by the *interannual variability* of river discharges are negligible. This is because the fresh river waters can significantly alter the stratification of the ocean in the bay compared to the stratification in the solution that excludes the rivers [Eq. (1); Han et al. 2001], whereas their less than 24% variabilities only slightly modify the stratification compared to the stratification in the solution that includes the climatological rivers and therefore resulting in a small SLA.

Effect of heat fluxes $+ P - E$ generally causes a SLA of $\lesssim$2 cm (thin dashed lines in Figs. 8a–c). During some years, however, SLAs due to this mechanism can be 2–5 cm, especially in the northern and western bay (Figs. 8b, c). In these two regions, SLAs produced by heat fluxes $+ P - E$ tend to be opposite to the SLAs generated by the bay wind (cf. the thin solid and thin dashed lines), and this opposite relationship is confirmed by the negative correlation of -0.47 in the northern bay and -0.33 in the western bay between SLAs due to the two mechanisms. Solutions from a new set of experiments designed to assess the influence of radiation and atmospheric fields (not shown) suggest that SLAs caused by the heat fluxes result from variabilities of atmospheric fields, and the effect of solar shortwave radiation and outgoing longwave radiation is negligible. While a strong northeast (southwest) monsoon tends to increase coastal downwelling (upwelling) so as to increase (decrease) h_1 and therefore raise (decrease) sea level [Eq. (1); section 4c], it brings more cold and dry (warm and humid) air into the bay, increasing (decreasing) evaporation and turbulent heat fluxes into the atmosphere and reducing (increasing) the SST, resulting in a sea level decrease (increase).

On the other hand, an increased alongshore wind speed during the southwest monsoon tends to increase latent and sensible heat fluxes and therefore acts to further decrease the low sea level produced by the increased coastal upwelling. Additionally, anomalous precipitation can modify the sea level by as much as 1 cm (not shown). All of these effects contribute to the SLAs shown by the thin dashed lines in Figs. 8a–c. Generally, SLAs caused by heat fluxes $+ P - E$ are weakly correlated with solution MR, with correlation coefficients of $\lesssim$0.25 in most regions except for the western bay where the correlation is -0.41 (Table 1) and deviation ratio is 0.26. That is, heat fluxes $+ P - E$ tends to reduce the amplitude of SLAs in the western bay.

Since our 4½-layer model is fully nonlinear, the system has a nonlinear response to each forcing. The MR SLAs are close to the sum of the SLAs due to each mechanism (not shown), suggesting that nonlinear response of the system to each forcing is not large.

2) BAY INTERIOR

In the interior bay (regions 4–5 of Fig. 7), amplitudes of sea level interannual variability are 5–15 cm (Figs. 9a,b), comparable with the SLAs along the coasts. In the central bay (Fig. 9a), equatorial wind forcing plays a control role, with a correlation of 0.86 and standard deviation ratio of 0.71 with the MR (Table 1). The bay wind, however, also has a significant effect, with a correlation coefficient of 0.56 and deviation ratio of 0.44 with the MR, especially during winter and spring. In the southwestern bay (Fig. 9b), the bay and the equatorial wind are equally important in causing the SLAs, with correlation coefficients of 0.50 and 0.54 and deviation ratios of 0.84 and 0.75 with the MR, respectively. During the southwest monsoon, forcing by the Bay wind dominates the equatorial wind, with a correlation of 0.60 and deviation ratio of 0.91 for the bay wind in comparison with 0.38 and 0.60 for the equatorial wind.

As to their effects along the coasts, the influence of rivers is negligible and the effect of heat fluxes $+ P - E$ is generally smaller than 2 cm in the bay interior.

3) WINDS

The above discussions demonstrate that sea level variability in the bay results predominantly from wind variability: The total effect of the bay and equatorial wind has a correlation of 0.913–0.977 and deviation ratio of 0.89–1.05 with solution MR (Table 1). Variabilities of wind in the bay and at the equator, however, are not completely independent. SLAs forced by the bay and equatorial wind, therefore, are significantly correlated. During summer and fall when the bay wind has a strong influence near the western boundary and in the southwestern bay, correlations between the SLAs in the eastern equatorial ocean (2°S–2°N, 90°–97°E) caused by the equatorial wind and SLAs produced by the bay wind are 0.59 during summer and 0.49 during fall along the western boundary, and -0.40 and -0.44 in the south-

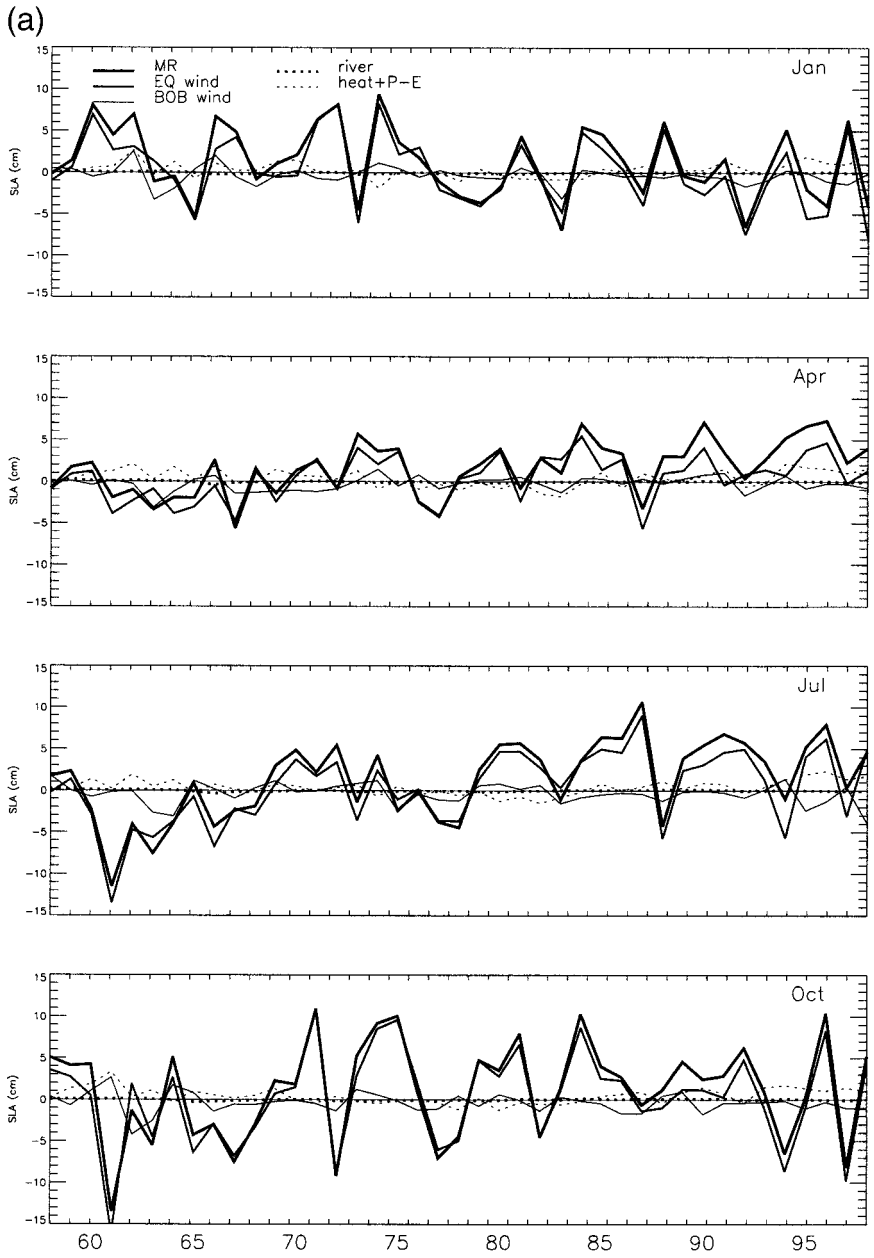

FIG. 8a. SLAs in the eastern bay (region 1 of Fig. 7) from solution MR (thick solid curves), and from solutions forced by variabilities of the equatorial wind (medium solid curves), the bay wind (thin solid curves), rivers (thick dashed curves), and heat fluxes $+ P - E$ (thin dashed curves) during Jan, (top), Apr (upper middle), Jul (lower middle), and Oct (bottom). Units for SLAs are cm.

western bay. In the northern bay, the corresponding correlations are 0.42 during summer and 0.50 during fall.

These correlations suggest that, when an easterly wind anomaly occurs in the equatorial ocean, a negative wind curl tends to appear in the southern bay and an upwelling favorable alongshore wind tends to appear along the western and northern boundaries. The anomalous easterly wind produces a negative SLA in the eastern equatorial ocean, the negative wind curl in the southern bay generates a positive SLA in the southwestern bay, and the upwelling favorable alongshore wind causes a negative SLA near the northern and western boundaries. This anomalous wind pattern suggests that variabilities of winds in the equatorial Indian Ocean and in the bay can be linked by a large-scale atmospheric system. In fact, this wind pattern is consistent with the

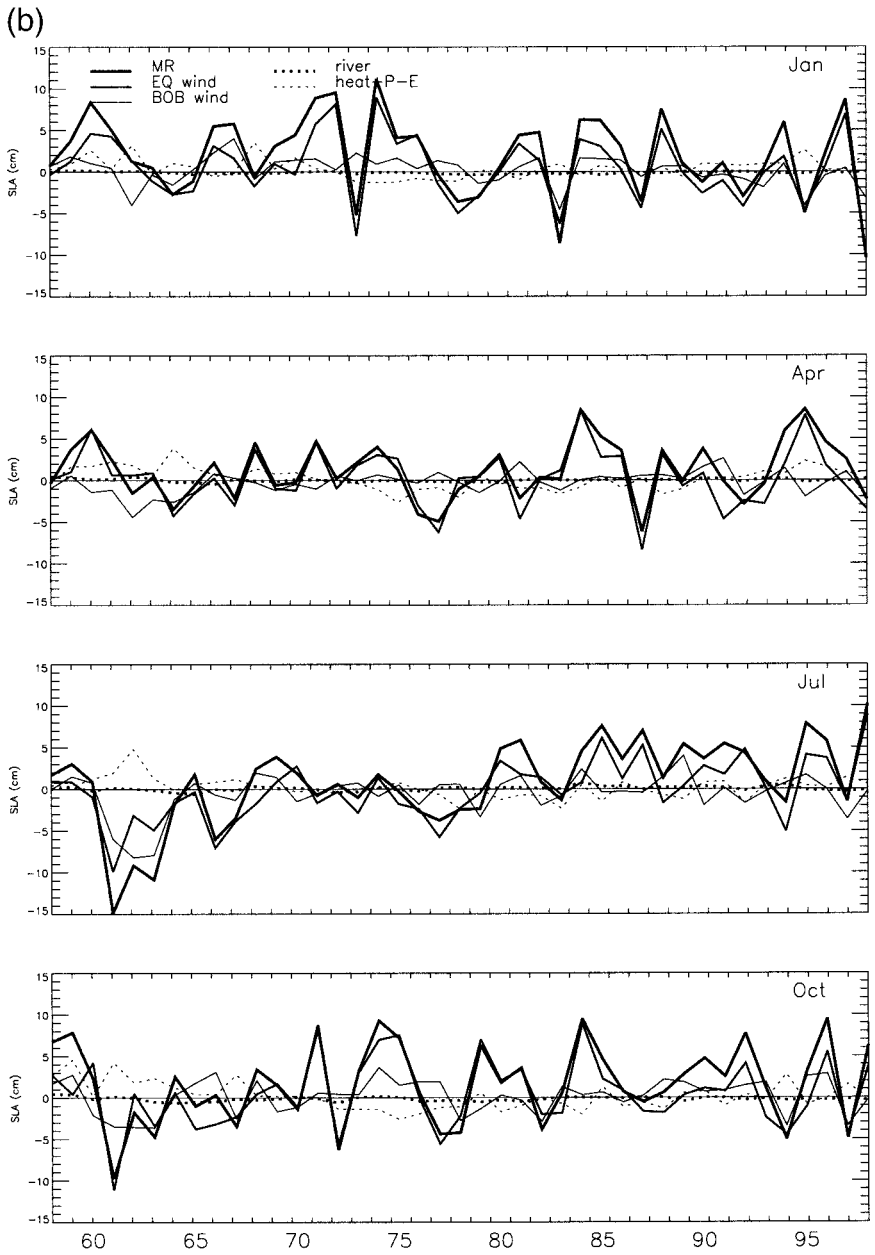

FIG. 8b. Same as in Fig. 8a except for the northern bay (region 2 of Fig. 7).

wind variability during positive dipole years (Fig. 2 of Saji et al. 1999), and is displayed in the top panels of Fig. 10a (section 4c). During a negative dipole, the wind pattern tends to reverse (bottom right panel of Fig. 10a).

c. Dynamics

Given the dominance of wind in causing sea level interannual variability in the bay, in this section we discuss the physical processes through which wind variability produces the sea level changes. Along the basin boundaries of the north Indian Ocean, dynamics of the wind-driven sea level variability at seasonal and interannual timescales have been discussed by Clarke and Liu (1993, 1994). Throughout the bay the physical processes that generate sea level change at seasonal timescale have been demonstrated by McCreary et al. (1996). Here, then, we only provide a brief discussion.

The case chosen to display the solution is the negative dipole of 1998, which follows the positive dipole of 1997 (Fig. 4). During 1998, a severe Bangladesh flooding happens during summer, and a high percentage of cholera occurs during fall.

Figure 10a shows the anomalous wind stress (arrows)

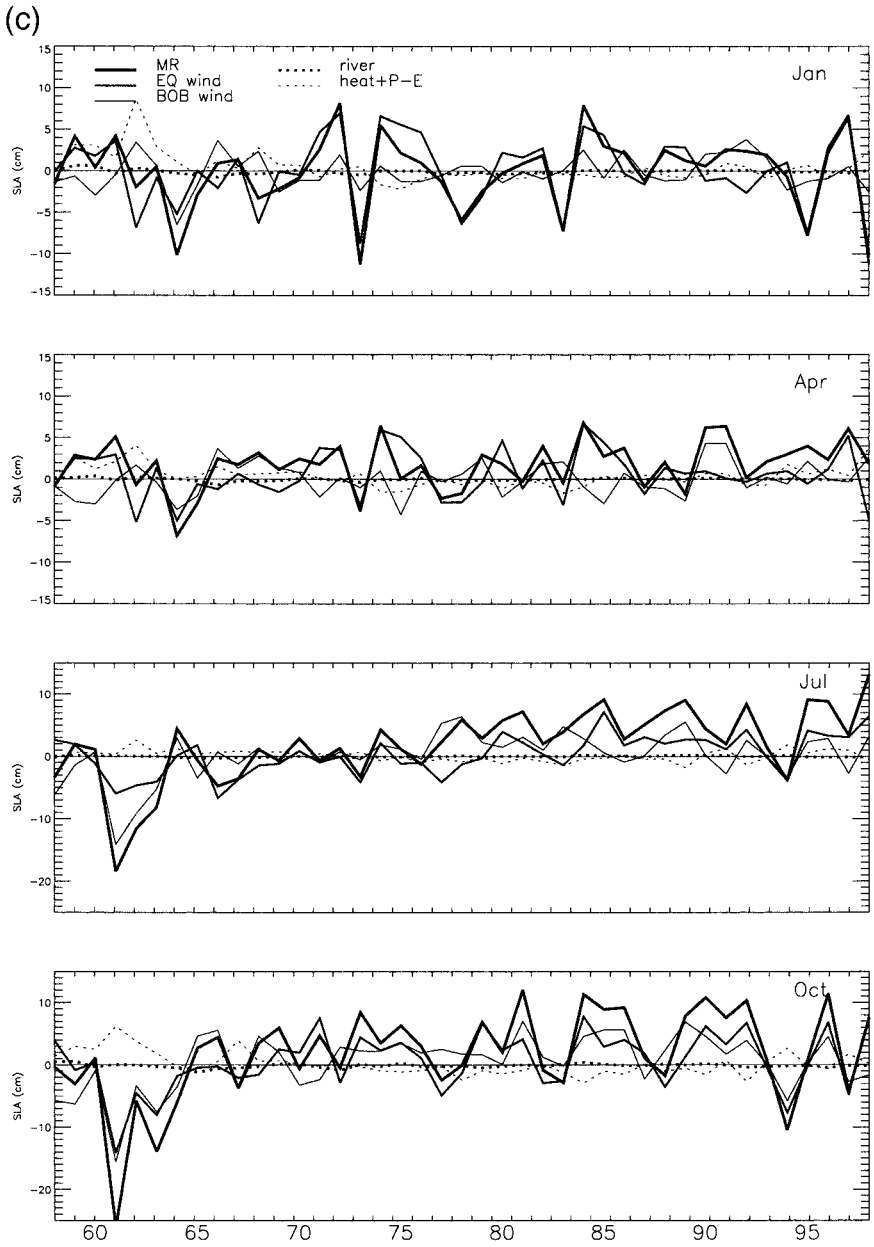

FIG. 8c. Same as in Fig. 8a except for the western bay (region 3 of Fig. 7). Note that the minimum scale is changed from −15 to −25 cm in Jul and Oct.

and curl (shades and contours) during August and November 1997 (top) and during February, May, August, and November 1998 (middle and bottom). Figure 10b shows the SLAs during August (left) and November (right) 1997 from solution MR (top), and from solutions forced by variabilities of equatorial wind (middle) and the bay wind (bottom).

During August 1997, the easterly wind anomaly in the equatorial ocean (top left of Fig. 10a), which is associated with the dipole mode event of this year, drives an equatorial divergence, shallows the thermocline, and results in a low sea level in the eastern equatorial ocean (middle left of Fig. 10b; Webster et al. 1999; Saji et al. 1999; Murtugudde et al. 2000). This low sea level signal strengthens and attains its maximum amplitude of 14–16 cm in November (middle right), when the anomalous equatorial wind associated with the dipole reaches its peak (top right panel of Fig. 10a). The negative SLAs in the eastern equatorial ocean propagate into the bay as coastal Kelvin waves along the eastern boundary, where they also radiate westward as Rossby waves, causing negative SLAs along the bay boundaries and in the interior bay. The positive SLAs in the central and southwestern bay (middle panels of Fig. 10b) result from

TABLE 1. Correlation coefficients between SLAs from solution MR and from solutions caused by interannual variability of the equatorial wind, the bay wind, total wind, heat fluxes + $P - E$, and the bay rivers, respectively. The correlation is based on monthly SLAs for the period 1958–98, and the coefficients are calculated for the eastern, northern, western, central, and southwestern bay. All correlations have a significance level of above 99.5%, except for the effect of heat fluxes + $P - E$ in the eastern bay, where the significance level is above 95%. Ratios of standard deviation are listed in the brackets for each mechanism in each region, and they are calculated by $S_r = S_1/S_0$, where S_1 and S_0 are the standard deviations for SLAs forced by a specific mechanism and for SLAs in solution MR, respectively.

	Solution MR				
Mechanism	Eastern	Northern	Western	Central	Southwestern
Equatorial wind	0.95 [0.95]	0.93 [0.85]	0.82 [0.75]	0.86 [0.71]	0.54 [0.75]
Bay wind	0.28 [0.26]	0.57 [0.40]	0.71 [0.59]	0.56 [0.44]	0.50 [0.84]
Total wind	0.977 [0.998]	0.972 [1.05]	0.975 [1.05]	0.962 [0.89]	0.913 [0.90]
Heat fluxes + $P - E$	−0.07 [0.21]	−0.24 [0.29]	−0.41 [0.26]	0.15 [0.24]	0.21 [0.31]
Rivers	0.11 [0.02]	0.14 [0.05]	0.13 [0.05]	0.16 [0.04]	0.27 [0.03]

the westward propagation of Rossby waves associated with the positive SLAs, which are produced by the equatorial westerly wind anomaly during the negative dipole of 1996 and strengthened somewhat during May of 1997 (not shown).

Meanwhile, the negative wind curls in the southern bay from August to November force westward propagating Rossby waves associated with positive SLAs in the southern, especially in the southwestern, bay during November (bottom panels of Fig. 10b). Although weak, the upwelling-favorable alongshore winds during September and October (not shown) strengthen the coastal upwelling and generate negative SLAs along the bay boundaries, with the maximum amplitude occurring at the western boundary due to the counterclockwise propagation of coastal Kelvin waves. In addition, the weak positive wind curls in the central and northern bay produce negative SLAs in the bay interior. SLAs in solution MR (top panels of Fig. 10b) are generated primarily by forcing due to the equatorial and the bay winds.

During February of 1998 (Fig. 10c), negative SLAs in the bay result mostly from the cyclonic propagation of coastal Kelvin waves and westward propagation of Rossby waves associated with the negative SLAs, which are produced during the positive dipole event of 1997. SLAs forced by the bay wind are negative in the south due to the westward propagating Rossby waves generated by the positive wind curl in the southeastern bay (middle left panel of Fig. 10a). In the central and southwestern bay, negative wind curl causes a high sea level, contributing to the positive SLAs in the MR.

In May, the negative SLAs in the eastern bay during February propagate to the central–western bay via Rossby waves (top and middle panels of Fig. 10c), and positive SLAs present in the eastern and northern bay. The high sea level signals are associated with coastal Kelvin waves forced by the westerly wind anomaly in the equatorial ocean (middle right panel of Fig. 10a). The bay wind generates negative SLAs in the southern and northwestern bay, owing to the positive wind curl in these regions. In the southwestern bay, SLAs are positive, and they are driven by the negative wind curl and the weak downwelling favorable wind along the east coast of India.

At the peak of the southwest monsoon, SLAs are positive throughout the bay (top left panel of Fig. 10d). This is because the positive SLAs generated in the equatorial ocean in May propagate westward as Rossby waves and counterclockwise as coastal Kelvin waves. At the same time, the equatorial signals are modified by the anomalous equatorial wind during May–August, producing the complicated pattern of SLAs (middle left). In addition, nonlinear response of the system to variability of the equatorial wind might also contribute to the complication. Negative wind curl in the central-western bay and downwelling favorable wind along the east Indian coast (bottom left panel of Fig. 10a) produce positive SLAs in the central and western bay (bottom left panel of Fig. 10d), strengthening the SLAs in the central and western basin. The upwelling favorable wind along the eastern boundary generates negative SLAs and therefore weakens the sea level changes in the eastern bay.

During November, SLAs are positive in the entire bay as they are in August (top right panel of Fig. 10d). Signals from the equatorial ocean weaken somewhat in the bay interior, owing to the relaxation of zonal pressure gradient at the equator during September and October, but strengthen somewhat in the northern bay due to the westward propagation of Rossby waves and alongshore propagation of coastal Kelvin waves generated by the strengthened equatorial westerly during November, which is associated with the negative dipole event (middle right panel of Fig. 10d and bottom right panel of Fig. 10a). The high sea level signals produced by the bay wind in August persists until November in the central–western bay. The SLA along the east coast of India, however, becomes negative due to the forcing of positive wind curl and upwelling favorable wind in the western bay.

In summary, along the eastern and northern boundaries of the bay, SLAs are predominantly produced by coastal Kelvin waves that propagate into the bay from the equatorial ocean and, to a much lesser degree, by the local alongshore wind that generates anomalous coastal upwelling. Along the western boundary, sea level variabilities are caused by both the equatorial wind and the bay wind. SLAs produced in the equatorial

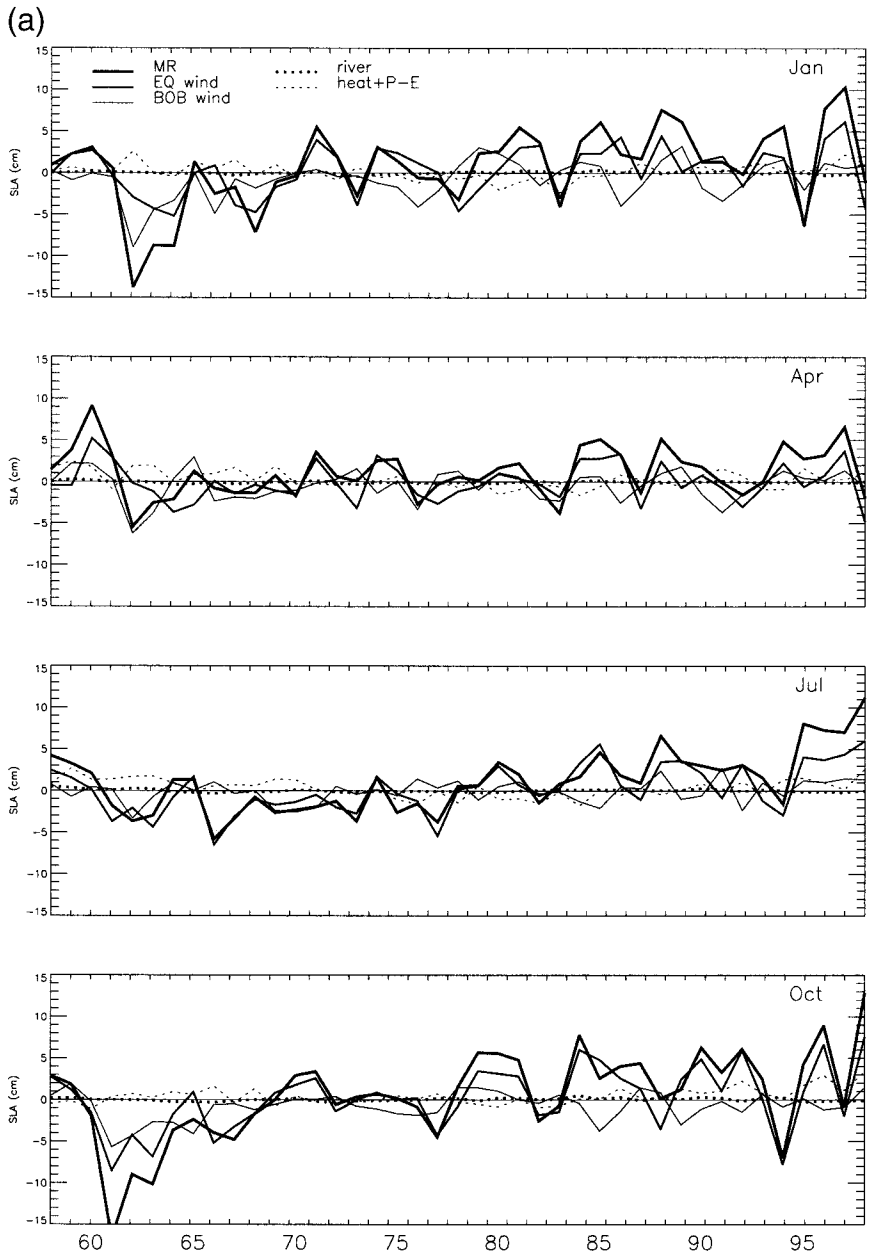

FIG. 9a. Same as in Fig. 8a except for the central bay (region 4 of Fig. 7).

ocean can influence the sea level in the western bay via both coastal Kelvin waves (fast: 27 days to reach 15°N at the west coast for $n = 2$ mode) and westward propagating Rossby waves with $C_r = \beta c^2/f^2$ cm s^{-1} (slow: 14.5 months to arrive at the same location for $n = 2$ mode), given the typical characteristic speeds of $c_1 = 264$ cm s^{-1} and $c_2 = 167$ cm s^{-1} for the first ($n = 1$) and second ($n = 2$) baroclinic modes in the Indian Ocean (Moore and McCreary 1990). In our model, characteristic speed for $n = 1$ mode is 335 cm s^{-1}, faster than its typical value, and the speed for the gravest $n = 2$ mode is 166 cm s^{-1}, close to its typical value. SLAs generated by the bay wind can be strong in the western bay, and their amplitudes increase toward the south due to the counterclockwise propagation of coastal Kelvin waves. In fact, the counterclockwise propagation of coastal Kelvin waves explains the increasing importance of the bay wind from the eastern via northern to the western bay discussed in section 4b(1), and the weaker effect of the bay wind in the eastern and northern bay contributes to the dominance of equatorial wind forcing in these regions.

In the bay interior, SLAs are caused by Rossby waves radiating westward from the eastern boundary, which

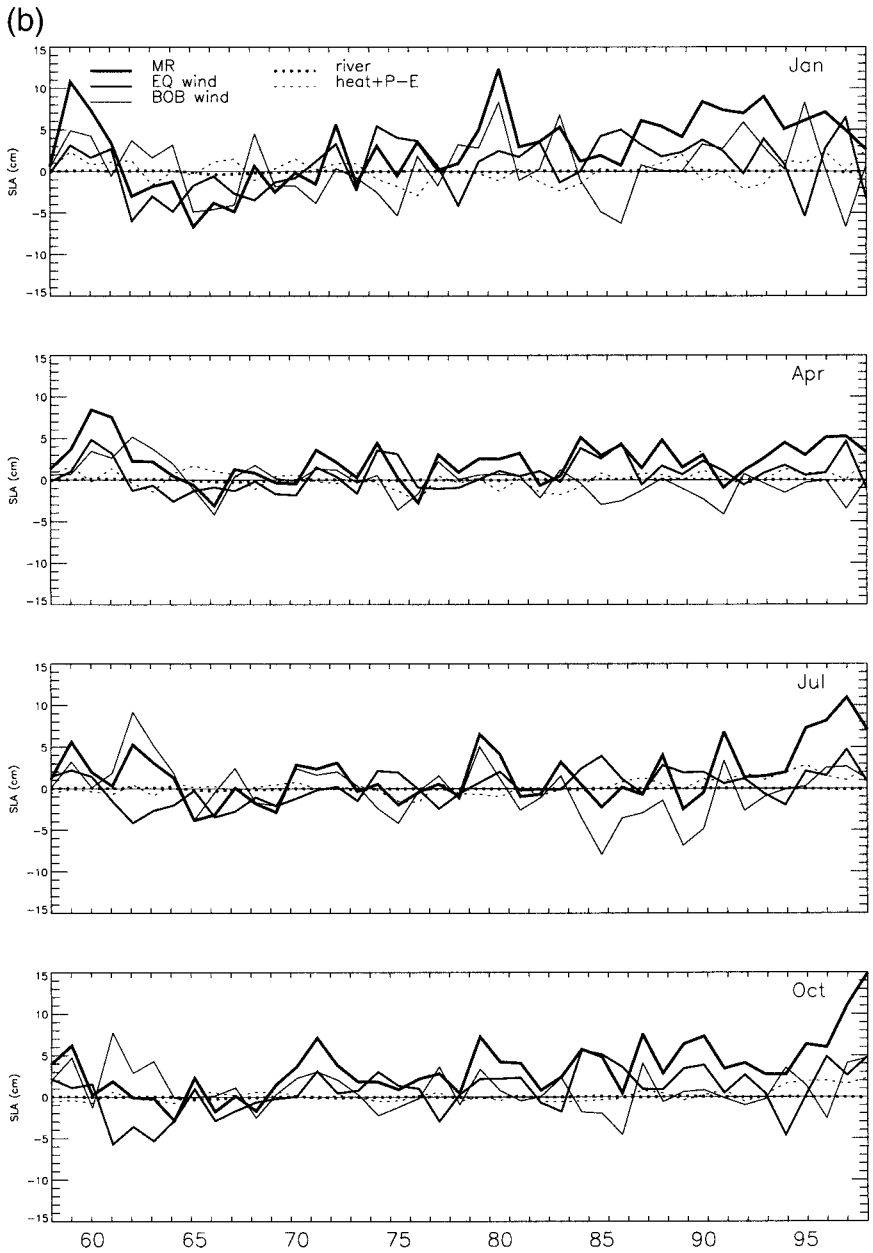

FIG. 9b. Same as in Fig. 8a except for the southwestern bay (region 5 of Fig. 7).

are originated from the equatorial ocean, and Rossby waves forced by the interior wind curl. The maximum influence of the bay wind is in the southwestern bay, because of the westward propagation of Rossby waves forced by the large-scale wind curl in the interior bay.

d. Interannual to decadal spectral peaks

Oscillation of SLAs at interannual timescale can be readily seen in Figs. 8a–c and 9a–b. To quantitatively determine the dominant periods for the oscillation, Fig. 11 shows the variance spectra for SLAs from solution MR (thick solid curves) in the northern (top left), western (top right), central (bottom left), and southwestern bay (bottom right). The spectrum in the eastern bay is not shown, since it is almost identical to that of the northern bay. In addition, spectrum for the observed SLAs at station Vishakhaptnam for the period of 1958–89 is plotted by the thick dashed curve in the top left panel.

In the northern bay two distinctive spectral peaks, with one located at 4–5 yr and the other at 13–14 yr period, present in both our MR solution and the observation. The 4–5 yr oscillation is above the 95% signif-

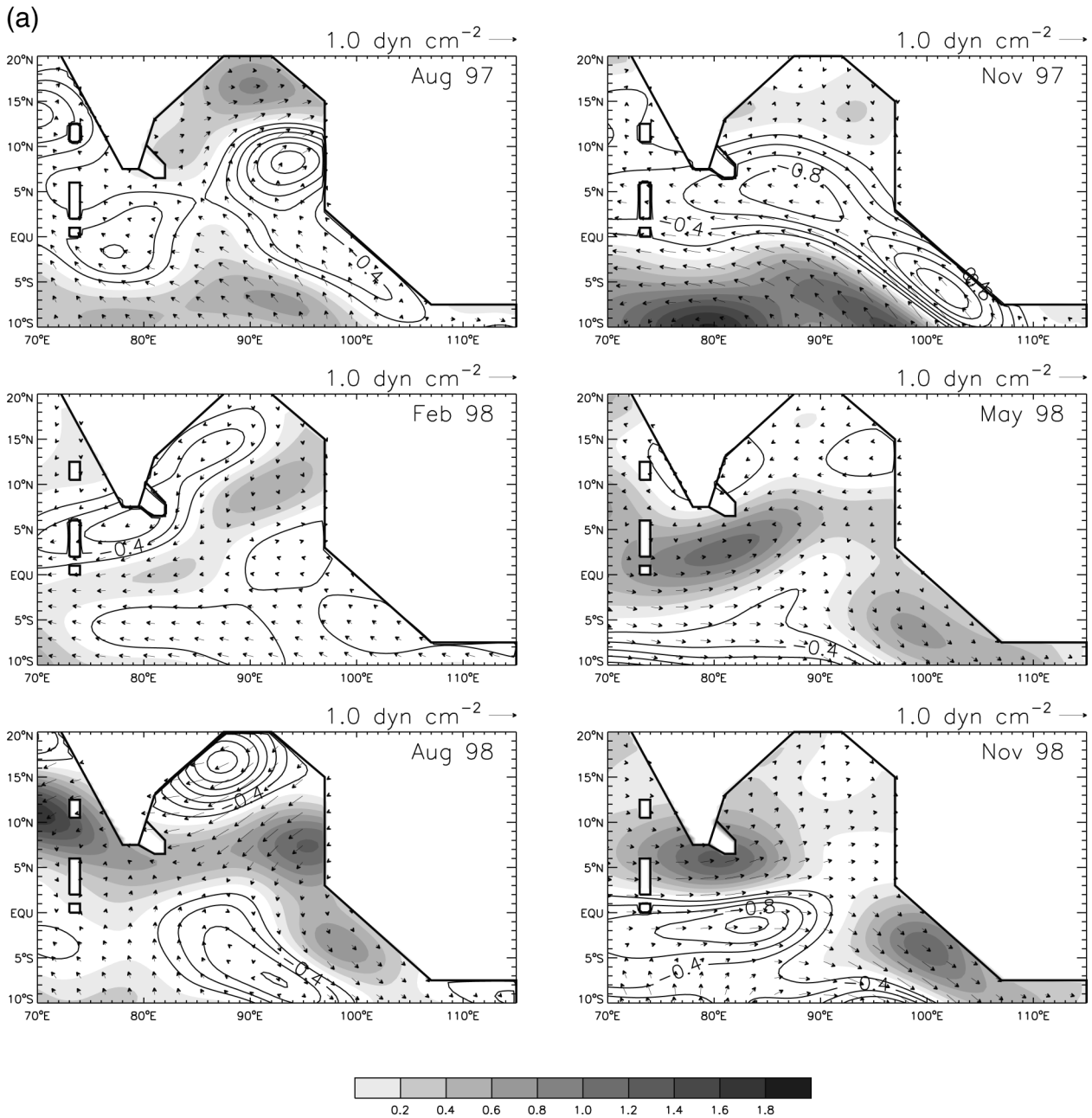

FIG. 10a. Anomalous wind stress (arrows) and curl (shades and contours) for Aug and Nov 1997 (top) and Feb, May, Aug, and Nov 1998, (middle and bottom). Calibration vector for wind stress of 1.0 dyn cm^{-2} is plotted above each panel. Positive wind curls are shaded and negative ones are contoured, with an interval of 0.2×10^{-8} dyn cm^{-3}.

icance level for both the model (thin solid line) and the data (thin dashed line), whereas the 13–14 yr peak is over 90% significance level only for the data (not shown). The lack of significance for the 13–14 yr peak is likely because of the short lengths of records (41 years for the model and 32 years for the data). On the other hand, the over 90% significance level for the data suggests that signals of decadal variability are strong during the data period. Additionally, peaks at 7 and 3.5 yr also exist in the observation, each of which exceeds 95% significance. Signatures of these secondary peaks present in our model, except that the periods appear to shift to 4 and 8 yr, respectively. In fact, the strongest 4–5 yr peak also has a halfyear shift, with 4.5 yr for the observation and 5 yr for the model. The model/data discrepancies might result from errors in the model and its forcing fields.

In the western and central bay, the near 5 and 13–14 yr peaks persist with somewhat weaker amplitudes in our solution, and the secondary peak of 7–8 yr is stron-

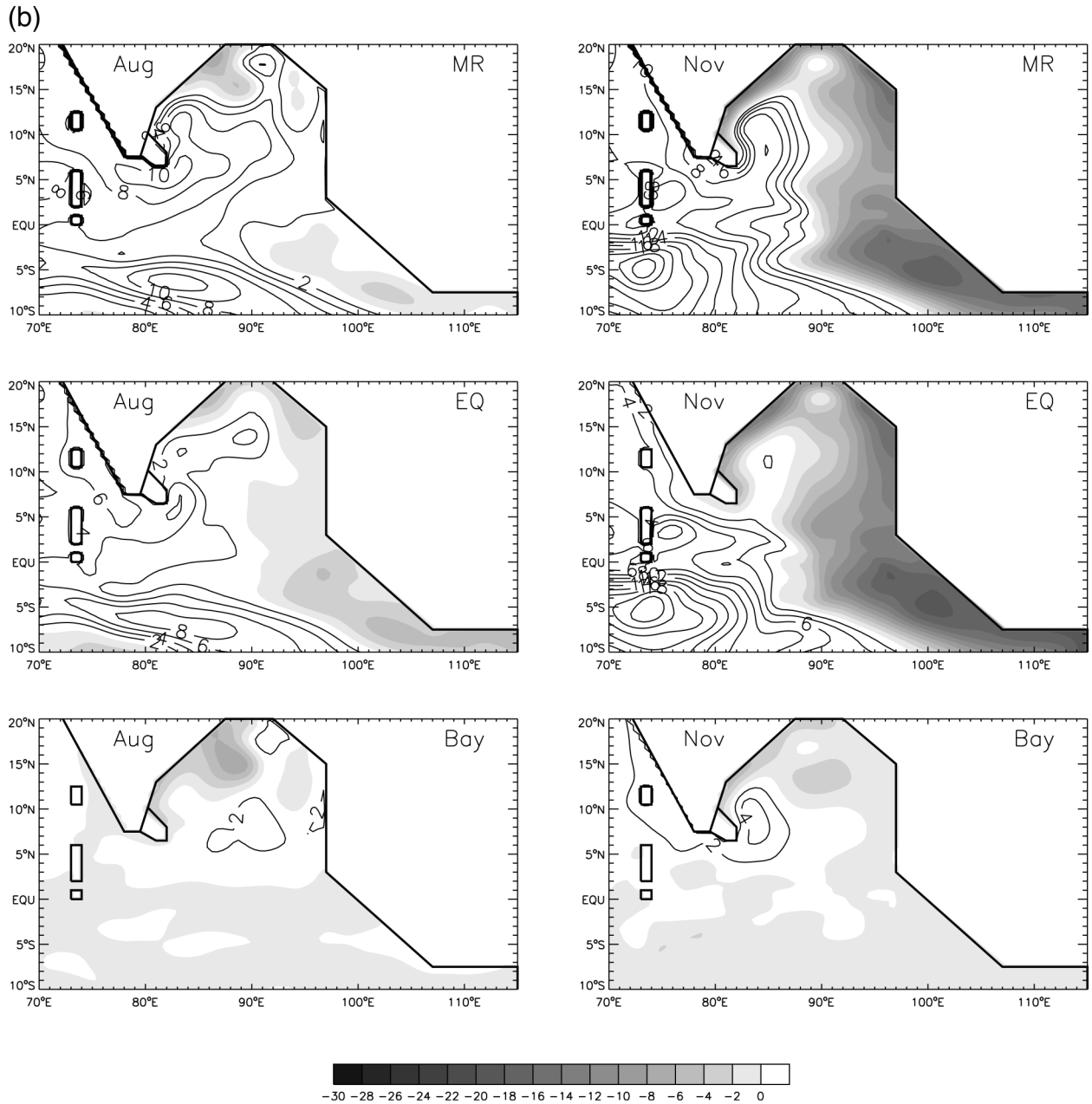

FIG. 10b. SLAs for 1997 from solution MR (top) and from the solutions forced by (middle) equatorial wind variability and (bottom) the bay wind variability during Aug (left) and Nov (right). Positive values are contoured and negative ones are shaded, with an interval of 2 cm.

ger than it is in the northern bay. The near 4-yr peak also exists, and it exceeds the 95% significance in our solution. Interestingly, a near biennial peak of 2.8-yr period occurs in the western bay with a significant power, and this peak, in fact, occurs in the northern and central bay with weaker amplitudes in our solution. This quasi-biennial oscillation, however, does not seem to appear in the data near the northern bay (top left), for a reason that is not clear. In the southwestern bay, the 4-yr and a near 10-yr peaks dominate the spectra.

Figure 11 suggests that sea level variability has multi-timescales, from interannual to decadal. Variabilities at interannual (2.8, 4, and 5 yr) and decadal timescale of 14 yr are dominated by the equatorial wind forcing (not shown), whereas variations at intradecadal (7–8 yr) and decadal timescale of 10 yr are predominantly caused by the bay wind (not shown). The 2.8-yr peak might be a signature of the tropical biennial oscillation, and the 4–5 yr peak might indicate the influence of ENSO. Understanding the dynamics that cause the interannual to decadal sea level variabilities is out of the scope of this paper, but is an important topic for our further research.

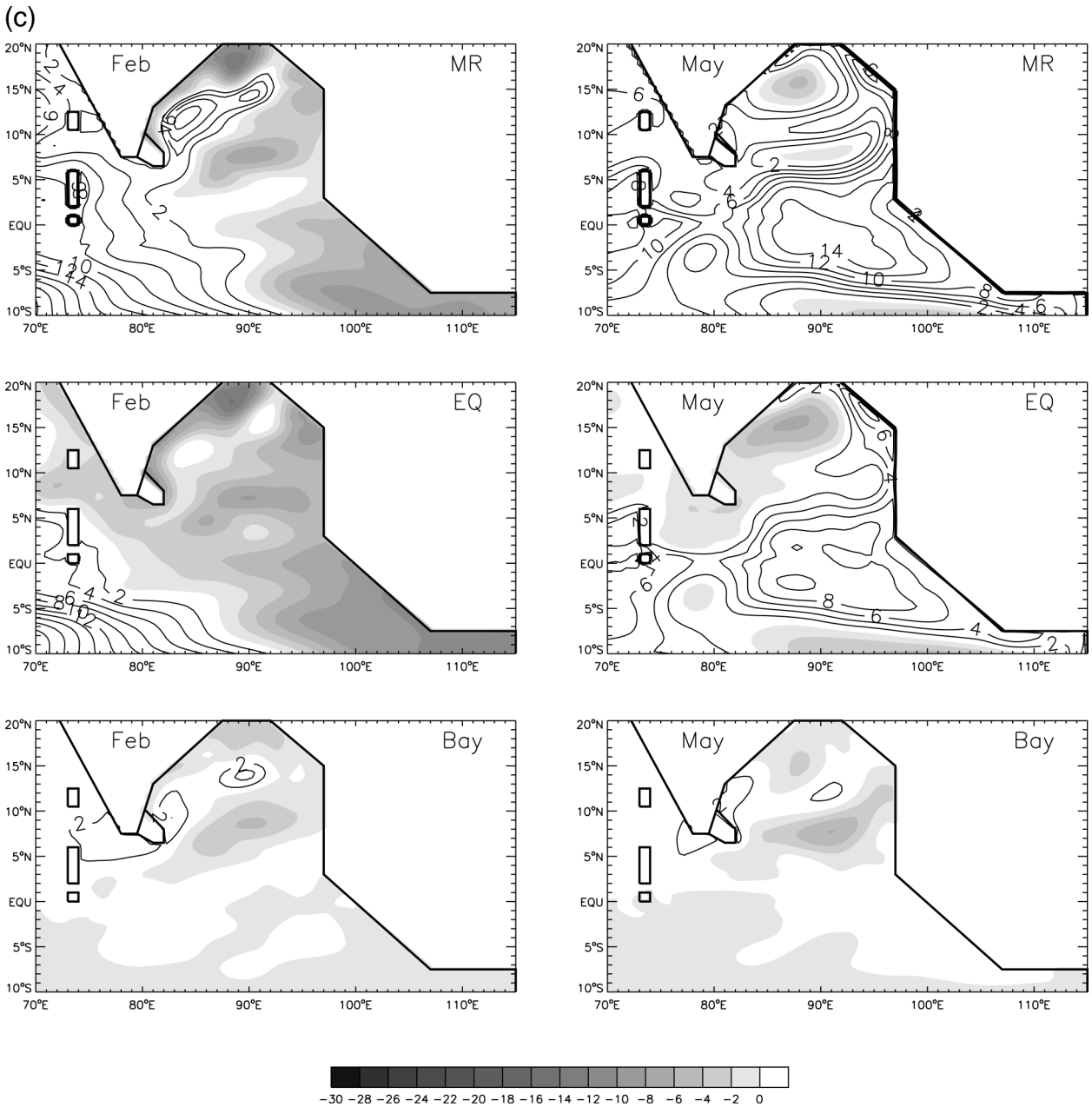

FIG. 10c. Same as in Fig. 10b except for Feb and May of 1998.

While Shankar and Shetye (1999) indicated the importance of monsoon rainfall in causing interdecadal variability of sea level along the west coast of India, our solutions suggest the dominant influence of variability of the equatorial and the bay wind in forcing the interannual to decadal sea level changes in the bay.

e. Potential application

It is suggested from our solutions that SLAs in the northern bay can last for the entire monsoon season or longer (Figs. 8b, 10b, and 10d). This low-frequency sea level variability might potentially play some role in haltering the river waters from flowing into the bay and influencing the Bangladesh flooding at interannual timescale. On a shorter timescale, a generally 10 cm sea level variability may be insignificant in aggravating the storm surges, which can cause meters of sea level changes. Taking into account the annual cycle, which attains the highest sea level of about 8 cm during the southwest monsoon season (Fig. 6), the total of approximately 20 cm SLA might be of some importance in favoring the flooding on both the longer and shorter timescales during the southwest monsoon.

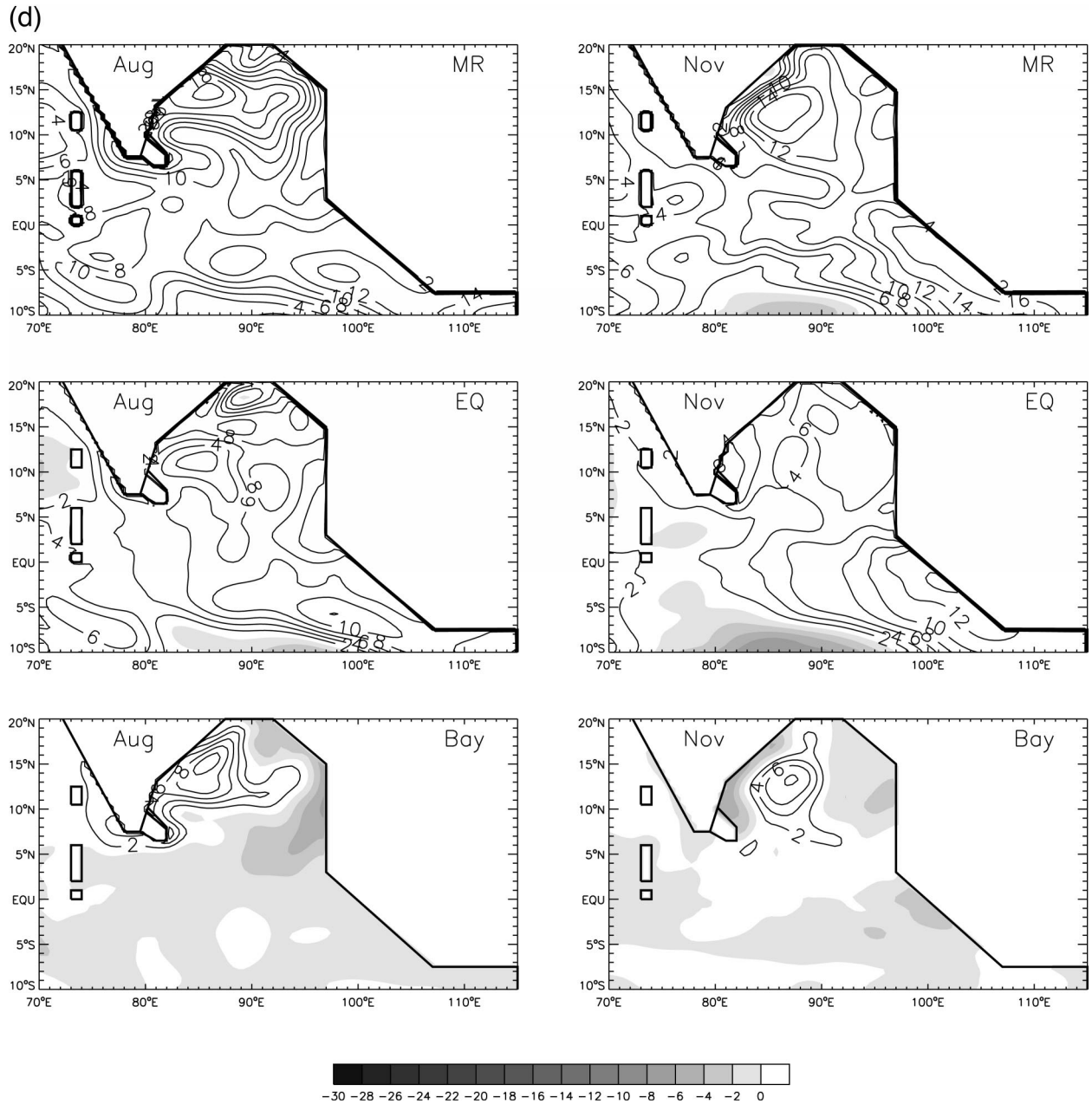

FIG. 10d. Same as in Fig. 10c except for Aug and Nov.

Cholera in Bangladesh generally occurs twice a year: spring and fall (Lobitz et al. 2000). A 10 cm sea level increase may play some role in increasing the inland incursion of plankton-laden water in Bangladesh, which is at or slightly above the sea level. It is hypothesized that zooplankton, that is, copepods, is a carrier of bacterium, V. cholerae, the bacterium that causes cholera (Lobitz et al. 2000). A positive correlation between the sea level anomaly and the percent of persons positive for cholera is suggested by Lobitz et al. (2000). They argued that the anomalously high sea level in the northern bay during summer and fall of 1998 and low sea level for the same season of 1997 may partly account for the much higher (lower) cholera in 1998 (1997).

Given the dominant effect of equatorial wind variability in driving the SLAs in the northern bay, sea level changes in the eastern equatorial ocean, or alternatively westerly wind anomalies at the equator, may be a potential index for predicting Bangladesh flooding and cholera. For a typical value of 0.3 dyn cm^{-2} anomalous westerly wind stress in the central–eastern ocean (2°S–2°N, 75°–95°E) that persists for a month, sea level in the eastern equatorial ocean (2°S–2°N, 90°–97°E) can increase by 5–6 cm. That is, a 10–12 cm SLA can take

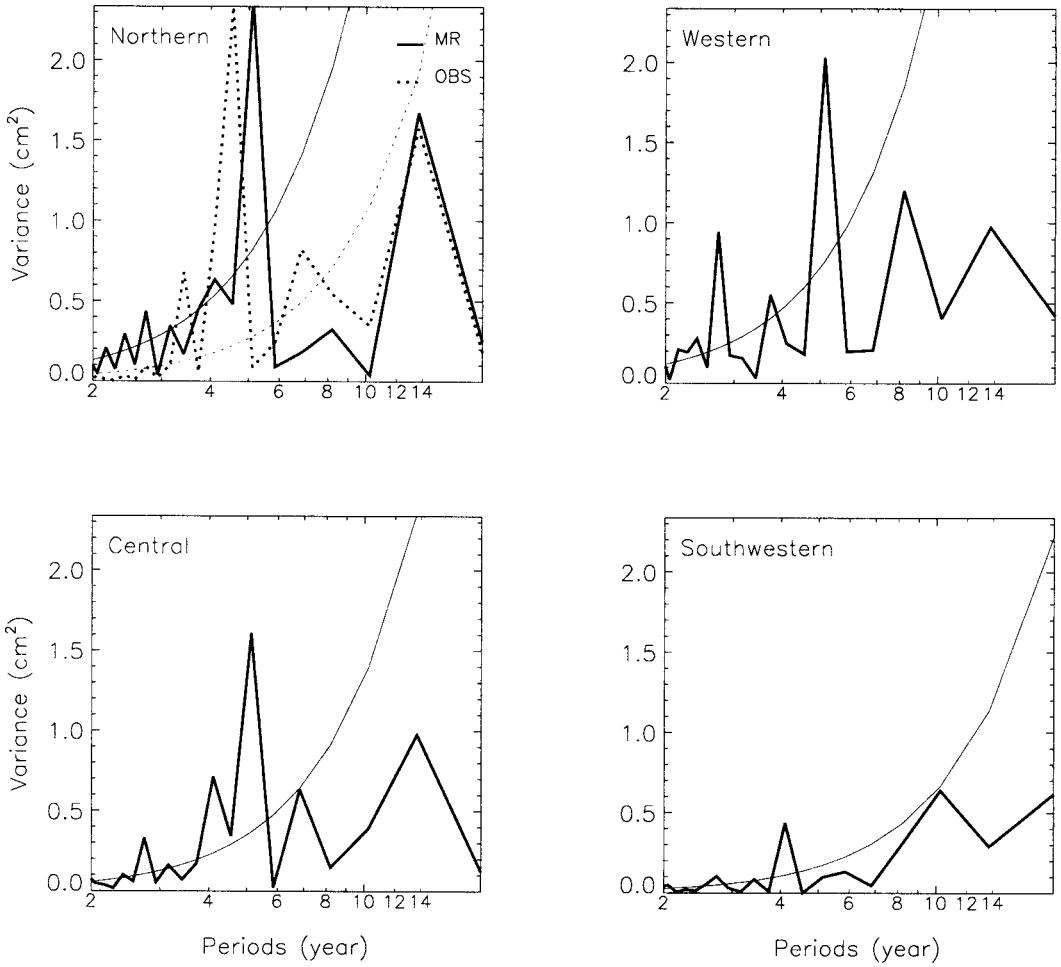

FIG. 11. Variance spectra for SLAs from solution MR (thick solid curves) based on the 41-yr results (1958–98) in the (top left) northern, (top right) western, (bottom left) central, and (bottom right) southwestern bay. The 95% significance level is plotted by the thin solid lines. Variance spectrum for SLAs from the tide gauge data based on the 32-yr record (1958–89) at station Vishakhaptnam is shown in the northern bay (top left, thick dashed curve), and its 95% significance level is shown by the thin dashed curve. Units for the variances are cm^2.

two months to build up. The correlation coefficient between the anomalous westerly wind of the present plus previous month and the anomalous sea level of the present month is 0.84. Since it takes approximately two weeks for $n = 1$ and three weeks for $n = 2$ mode coastal Kelvin waves to propagate from the equator to the northern bay for the typical characteristic speeds in the Indian Ocean (Moore and McCreary 1990), we can predict the low frequency SLAs in the northern bay about 3 weeks in advance. In fact, the correlation between the westerly wind anomalies (or SLAs) at the equator for the present plus previous month and the SLAs in the northern bay of the present month is 0.80 (0.87).

Since a strong positive SLA in the eastern equatorial ocean during summer and fall is generally associated with a negative dipole in the tropical Indian Ocean (Fig. 10d), a negative dipole event tends to enhance the flooding potential and aggravate the fall cholera in Bangladesh. In contrast, a positive dipole tends to reduce the chance of Bangladesh flooding and cholera. As discussed in section 4b(1), alongshore wind in the bay also has a significant influence in the northern bay during summer and fall, although its effect is not as strong as that of the equatorial wind. SLAs caused by the bay wind, however, tend to be positively correlated with those produced by the equatorial wind in the northern bay during the two seasons [section 4b(3)], suggesting that the alongshore wind tends to increase the amplitude of SLAs that generated by the equatorial wind.

5. Summary and discussion

In this paper a 4½-layer reduced-gravity ocean model is used to investigate the influence of the following four mechanisms in causing sea level interannual variability in the Bay of Bengal: interannual variability of river discharges into the bay, the local bay wind, the remote equatorial wind, and heat fluxes $+ P - E$. Solutions

are found in a basin that resembles realistic Indian Ocean north of 29°S (left panels of Fig. 3), and they are forced by NCEP–NCAR reanalysis fields from 1958 to 1998. Three major rivers are included: the Ganges–Brahmaputra, Irrawaddy, and Godavari. Due to the lack of river records, monthly discharges of the Ganges–Brahmaputra and Godavari during years of no observations within the period of 1958–98 are estimated by linear regression between their available observations and the NCEP precipitation in their catchments, respectively [section 2c(2) and Fig. 2]. Discharge for the Irrawaddy is chosen to be 40% of that for the Ganges–Brahmaputra.

A hierarchy of solutions are found to estimate the effect of each mechanism (section 2d). Solution MR includes all forcing mechanisms and is the most complete solution in the hierarchy. Results from this solution show reasonable agreements with the TOPEX/Poseidon altimetry data in the Indian Ocean (Fig. 3) and with the tide gauge data in the northern bay (Fig. 5). The good model/data agreements suggest that our model properly represents fundamental physics that determine sea level interannual variability both within and outside the bay.

Our solutions confirm the dominance of wind variation in driving sea level interannual variability [section 4b(3); Table 1], a conclusion suggested by earlier studies mentioned in the introduction. Results from this research also provide a clear picture for the influence of each mechanism on sea level interannual changes both along the coasts and in the bay interior. In addition, questions raised by previous studies on the influence of thermal and salinity forcings are quantitatively estimated.

SLAs produced by interannual variability of heat fluxes $+ P - E$ are generally small (thin dashed lines in Figs. 8a–c and 9a,b), with a maximum correlation of -0.41 in the western bay with solution MR (Table 1). In other regions, correlation coefficients for this effect are smaller than 0.24. Thus, heat fluxes $+ P - E$ tends to reduce the amplitudes of SLAs in solution MR in the western bay, with a standard deviation ratio of 0.26 relative to the MR. To a lesser degree, this effect acts to reduce the amplitudes of SLAs in the northern bay. The negative correlation results primarily from forcing by variability of the atmospheric variables, and effect due to solar shortwave and outgoing longwave radiations is negligible [section 4b(1)].

Although the amplitude of sea level annual cycle can increase by 15 cm in some regions of the bay by including the climatological bay rivers (Han et al. 2001), SLAs caused by interannual variability of river discharges are negligible (thick dashed lines in Figs. 8a–c and 9a,b; Table 1). This is because the fresh character of river waters significantly changes the stratification of the ocean relative to the solution excluding the rivers, therefore affecting the sea level markedly [Eq. (1); Han et al. 2001]. In contrast, the generally less than 25% interannual variability of river discharges [section 4b(1)] only slightly alters the stratification of the ocean compared to the solution that includes the climatological rivers, producing a negligible effect on interannual SLAs.

Along the coasts, influence of the equatorial wind is generally more important than the bay wind in causing SLAs, especially near the eastern and northern boundaries where effect of the former dominates the latter. Equatorial zonal wind anomalies produce SLAs especially in the eastern equatorial ocean due to the eastward propagation of equatorial Kelvin waves. Signals of these SLAs propagate into the bay as coastal Kelvin waves along the eastern boundary, where they also radiate westward into the bay interior as Rossby waves. Relative to solution MR, the importance of equatorial wind decreases counterclockwise along the coasts, from the east via north to the west coast of the bay (Table 1; thick solid and medium solid lines of Figs. 8a–c and 9a,b). This decrease results primarily from the increasing importance for the bay wind owing to the counterclockwise propagation of coastal Kelvin waves generated by the large-scale alongshore wind stress adjacent to the coasts. As a result, SLAs forced by the bay wind have comparable amplitudes to SLAs forced by the equatorial wind near the western boundary, especially during summer and fall when the anomalous alongshore wind attains large amplitudes. Note that signals forced by the equatorial wind also decrease while they propagate along the coasts due to damping. This decrease, however, is weak and cannot account for its decreasing influence discussed above. The dominance of equatorial wind forcing near the eastern and northern boundaries is consistent with Clarke and Liu (1994). In contrast, our solutions also suggest a comparable influence of the bay and equatorial wind forcing along the western boundary of the bay.

In the central bay, SLAs are produced primarily from the westward radiating Rossby waves generated by the equatorial wind variability (Fig. 9a; Table 1). In the southwestern bay, SLAs result equally from forcing due to the bay and equatorial wind (Table 1; Fig. 9b), and are dominated by the bay wind forcing during the southwest monsoon season [section 4b(2)]. The westward intensification of the bay wind influence is associated with the westward propagation of Rossby waves forced by the large-scale wind curl in the interior bay.

Interestingly, variability of the bay wind is not completely independent from variability of the equatorial wind, suggesting the equatorial–subtropical connection in wind variation [section 4b(3)]. SLAs in the eastern equatorial ocean are significantly correlated with the SLAs forced by the bay wind, with a positive correlation along the northern and western boundaries and negative correlation in the southwestern bay. The anomalous wind pattern that generates the correlations can be seen in the top panels of Fig. 10a (a positive dipole), and this pattern is better described by the composite anomalous wind plot during positive dipole events (Fig. 2 of

Saji et al. 1999). In fact, at the peak of the positive dipole in 1997, SLAs generated at the equator and produced by the bay wind are correlated as expected (middle right and bottom right panels of Fig. 10b). During the negative dipole of 1998 (bottom panels of Fig. 10a), the anomalous wind pattern tends to reverse compared to the positive dipole. Because of the independent components of the equatorial and the bay wind variabilities, the above correlations are not necessarily true for a specific case, such as during the fall of 1998, when the equatorial SLAs are positive, SLAs in the western bay are negative opposite to the suggested correlation.

Spectral analysis on SLAs in the bay shows several distinctive peaks (Fig. 11). In the order of periods they are at or near 2.8, 4, 5, 7–8, 10, and 13–14 yr. Except for the 7–8 and 10 yr peaks that are forced primarily by the bay wind, all other peaks result from equatorial wind forcing. The peaks with period shorter than 6 (12) yr are above the 95% (90%) significance level in both the data and the model, and the 13–14 yr peak is over (below) 90% significance in the data (model). Nevertheless, these spectral peaks might suggest the dominance of ENSO influence in the equatorial Indian Ocean (the strongest peak near 5 yr), effect of the tropical biennial oscillation (2.8 yr), and the strong signals of decadal (13–14 and 10 yr) and intradecadal (7–8 yr) oscillations in the Indian Ocean.

Finally, given the dominant influence of equatorial wind in causing SLAs in the northern bay, and the positive correlation between SLAs in the northern bay and percents of people positive for cholera in Bangladesh (Lobitz et al. 2000), sea level anomalies in the eastern equatorial ocean, or alternatively equatorial zonal wind variabilities, may serve as an index for predicting flooding and cholera in Bangladesh, which is at or slightly above the sea level. As pointed out in section 3, however, our model tends to underestimate the amplitudes of sea level variability during some years near the northern bay (Fig. 5). This model/data discrepancy might indicate the influence of continental shelf that is neglected in our model, which may modify the sea level signals that propagate to the northern bay as coastal Kelvin waves from the eastern equatorial ocean. Further understanding of the sea level influence on Bangladesh flooding and epidemic diseases requires examining the effect of continental shelf, which will be addressed in our further research. In addition, understanding the dynamics that cause the interannual to decadal sea level oscillations in the Indian Ocean will not only potentially contribute to predicting flooding and diseases in Bangladesh at interannual to decadal timescales, but also improve our understanding of monsoon variability and therefore potentially lead to improvement of the Asian–Australian monsoon prediction.

Acknowledgments. We thank D. Shankar for his helpful suggestions on using the Permanent Service for Mean Sea Level (PSMSL) and the two anonymous reviewers for their constructive comments for improving the manuscript. Appreciation also goes to the National Center for Environmental Prediction (NCEP) for making the forcing fields available on the Internet, and the Climate Diagnostics Center of NOAA for providing the anonymous FTP site of COADS surface atmospheric pressure. The authors were supported by NSF Grant ATM-9526030.

REFERENCES

Behera, S. K., R. Krishnan, and T. Yamagata, 1999: Unusual ocean–atmosphere conditions in the tropical Indian Ocean during 1994. *Geophys. Res. Lett.,* **26,** 3001–3004.

Clarke, A. J., and X. Liu, 1993: Observations and dynamics of semiannual and annual sea levels near the eastern equatorial Indian Ocean boundary. *J. Phys. Oceanogr.,* **23,** 386–399.

——, and ——, 1994: Interannual sea level in the northern and eastern Indian Ocean. *J. Phys. Oceanogr.,* **24,** 1224–1235.

Han, W., 1999: Influence of salinity on dynamics, thermodynamics, and mixed-layer physics in the Indian Ocean. Ph.D. dissertation, Library of the Oceanographic Center, Nova Southeastern University, 147 pp.

——, and J. P. McCreary, 2001: Modeling salinity distribution in the Indian Ocean. *J. Geophys. Res.,* **106,** 859–877.

——, J. P. McCreary, D. L. T. Anderson, and A. J. Mariano, 1999: On the dynamics of the eastward surface jets in the equatorial Indian Ocean. *J. Phys. Oceanogr.,* **29,** 2191–2209.

——, ——, and K. E. Kohler, 2001: Influence of precipitation–evaporation and Bay of Bengal rivers on dynamics, thermodynamics, and mixed layer physics in the upper Indian Ocean. *J. Geophys. Res.,* **106,** 6895–6916.

Huq, S., Z. Karim, M. Asaduzzaman, and F. Mahtab, Eds., 1999: *Vulnerability and Adaptation to Climate Change for Bangladesh.* Kluwer Academic, 147 pp.

Levitus, S., and T. P. Boyer, 1994: *World Ocean Atlas 1994,* Vol. 4: *Temperature,* NOAA Atlas NESDIS 4, 117 pp.

——, R. Burgett, and T. P. Boyer, 1994: *World Ocean Atlas 1994,* Vol.3: *Salinity,* NOAA Atlas NESDIS 3, 99 pp.

Lobitz, B., L. Beck, A. Huq, B. Wood, G. Fuchs, A. S. G. Faruque, and R. Colwell, 2000: Climate and infectious disease: Use of remote sensing for detection of Vibrio cholerae by indirect measurement. *Proc. Natl. Acad. Sci.,* **97,** 1438–1443.

McCreary, J. P., and P. K. Kundu, 1989: A numerical investigation of sea-surface temperature variability in the Arabian Sea. *J. Geophys. Res.,* **94,** 16 097–16 114.

——, ——, and R. L. Molinari, 1993: A numerical investigation of dynamics, thermodynamics, and mixed-layer processes in the Indian Ocean. *Progress in Oceanography,* Vol. 31, Pergamon, 181–224.

——, W. Han, D. Shankar, and S. R. Shetye, 1996: On the dynamics of the East India Coastal Current 2: Numerical solutions. *J. Geophys. Res.,* **101** (C6), 13 993–14 010.

Moore, D. W., and J. P. McCreary, 1990: Excitation of intermediate-frequency equatorial waves at a western ocean boundary: With application to observations from the Indian Ocean. *J. Geophys. Res.,* **95,** 5219–5231.

Murtugudde, R., J. P. McCreary, and A. J. Busalacchi, 2000: Oceanic processes associated with anomalous events in the Indian Ocean with relevance to 1997–1998. *J. Geophys. Res.,* **105** (C2), 3295–3306.

Perigaud, C., and P. Delecluse, 1993: Interannual sea level variations in the tropical Indian Ocean from Geosat and shallow water simulations. *J. Phys. Oceanogr.,* **23,** 1916–1934.

Potemra, J. T., M. E. Luther, and J. J. O'Brien, 1991: The seasonal circulation of the upper ocean in the Bay of Bengal. *J. Geophys. Res.,* **96,** 12 667–12 683.

Rao, R. R., R. L. Molinari, and J. F. Festa, 1989: Evolution of the

climatological near-surface thermal structure of the tropical Indian Ocean. Part 1: Description of mean monthly mixed-layer depth and sea-surface temperature, surface-current and surface meteorological fields. *J. Geophys. Res.*, **94** (C8), 10 801–10 815.

——, ——, and ——, 1991: Surface meteorological and near-surface oceanographic atlas of the tropical Indian Ocean. NOAA Tech. Memo. ERL AOML-69, 59 pp.

Reynolds, R. W., and T. M. Smith, 1994: Improved global sea surface temperature analyses *J. Climate*, **7,** 929–948.

Saji, N. H., B. N. Goswami, P. N. Vinayachandran, and T. Yamagata, 1999: A dipole mode in the tropical Indian Ocean. *Nature*, **401,** 360–363.

Shankar, D., and S. R. Shetye, 1999: Are interdecadal sea level changes along the Indian coast influenced by variability of monsoon rainfall? *J. Geophys. Res.*, **104** (C11), 26 031–26 042.

Shetye, S. R., 1993: The movement and implications of the Ganges–Brahmaputra run off on entering the Bay of Bengal. *Curr. Sci.*, **64,** 32–38.

UNESCO, 1993: Discharge of selected rivers of the world. *Studies and Reports in Hydrology*, Vol. 2, Part 2, UNESCO, 600 pp.

Webster, P. J., A. M. Moore, J. P. Loschnigg, and R. R. Leben, 1999: Coupled ocean–atmosphere dynamics in the Indian Ocean during 1997–1998. *Nature*, **401,** 356–360.

Yu, L., and M. Rienecker, 1999: Mechanisms for the Indian Ocean warming during the 1997–1998 El Niño. *Geophys. Res. Lett.*, **26,** 735–738.

——, and ——, 2000: Indian Ocean warming of 1997–1998. *J. Geophys. Res.*, **105,** 16 923–16 939.

——, J. J. O'Brien, and J. Yang, 1991: On the remote forcing of the circulation in the Bay of Bengal. *J. Geophys. Res.*, **96,** 20 449–20 454.